AD-A064 066 AIR FORCE INST OF TECH WRIGHT-PATTERSON AFB OHIO SCH--ETC F/G 20/12
PHOTOLUMINESCENCE OF GALLIUM INDIUM ARSENIC PHOSPHIDE.(U)
SEP 78 J G VARNI

UNCLASSIFIED AFIT/GEP/PH/78D-14 NL

1 OF 1
AD A064066

END
DATE FILMED
3-79
DDC

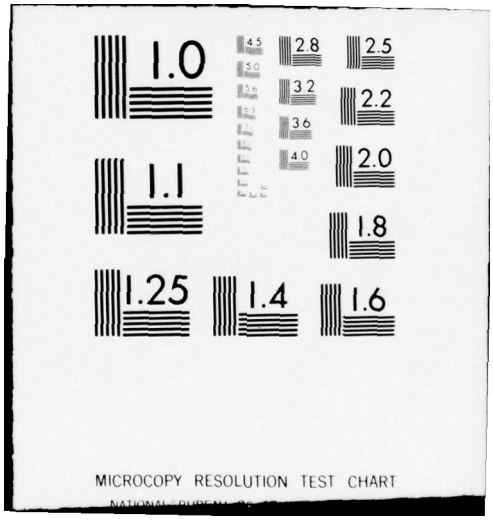
1.0
1.1
1.25
1.4
1.6
1.8
2.0
2.2
2.5
2.8
3.2
3.6
4.0
4.5
5.0
MICROCOPY RESOLUTION TEST CHART

LEVEL II

1

PHOTOLUMINESCENCE OF GALLIUM INDIUM ARSENIC PHOSPHIDE

THESIS

AFIT/GEP/PH/78D-14 Jamie G. G. Varni
2nd Lt USAF

Approved for public release; distribution unlimited

(14) AFIT/GEP/PH/78D- 14

(6) PHOTOLUMINESCENCE OF ~~GaInAsP~~ Gallium Indium Arsenic Phosphide.

THESIS (9) Master's thesis

Presented to the Faculty of the School of Engineering

of the Air Force Institute of Technology

Air University

in Partial Fulfillment of the

Requirements for the Degree of

Master of Science

by

(16) 2002 (12) 95 P.

(17) 07

(10) Jamie G. G. Varni ~~B.S.~~

2nd Lt USAF

Graduate Engineering Physics

(11) Sept~~ember~~ 1978

Approved for public release; distribution unlimited

012 225

slt

Preface

This report is the result of an attempt to see what impurity levels and defect levels were present in liquid phase epitaxy GaInAsP epilayers grown on InP substrates. Hopefully, the material contained herein will aid the Air Force Avionics Laboratory in their search for GaInAsP samples sufficiently pure, perfect, and thin (0.4 μm) to use in the construction of improved microwave devices.

I would like to express my gratitude to my thesis advisor, Dr. Theodore E. Luke, and to Dr. Robert L. Hengehold for their advice and aid in completing the project. Thanks are also due to James Miskimen, Ron Gabriel, and George Gergal. Without their constant help and technical advice this project could not have been finished.

For her indispensable moral support and enthusiasm tendered across vast distances, I dedicate this work to Diane Hamilton of Malibu, California.

Jamie G. G. Varni

Contents

Contents

List of Figures and Tables

Table — Page

Abstract

A photoluminescent study of high-purity epitaxial GaInAsP was made to determine what impurity and defect levels were present in the epilayers. The samples were excited with an argon-ion laser operating at 4880 Å and 700 mW of power or 4765 Å and 300 mW of power. Luminescence was detected with a cooled PbS photoconductor for sample temperatures from 4.2°K to 100°K. No defect-related peaks were found to be present in the samples. The emission spectrum of all of the samples was similar, consisting of a narrow, near-band edge peak and a broader peak between 15 meV and 26 meV below the band edge peak. The narrow peak was tentatively identified as being due to free-to-bound recombination. The broad peak was attributed to donor-acceptor pair emission, but no attempt was made to identify the impurities responsible for either peak.

PHOTOLUMINESCENCE OF GaInAsP

I. Introduction

Background

Interest in the quaternary solid solution Gallium Indium Arsenic Phosphide (GaInAsP) became intense in the early years of this decade. Researchers were searching for direct bandgap materials that could be lattice matched to the substrate on which they were grown. Lattice mismatch had been determined to be detrimental to the growth and the electrical and optical properties of the material (Refs 2:1574; 17:1). Specifically, lattice mismatch introduced non-radiative recombination centers that degraded optoelectronic device performance (Ref 1: 53) and formed electrically active defects at the substrate-epilayer interface of microwave devices (Ref 17:1).

In the late 1960's, researchers discovered that many III-V ternary solid solutions could be lattice matched to a given substrate material, but the growth procedures were difficult and could be successfully accomplished for only one value of lattice constant and bandgap per ternary alloy (Ref 2:1574). Then a team at Varian Associates discovered that by adding a fourth element to the solid solution, lattice matching could be achieved more easily and for a wide range of lattice constants and bandgaps (Ref 1:48). In particular, the quaternary solid solution $Ga_xIn_{1-x}As_yP_{1-y}$, where "x" is the molar

percentage of Ga and "y" the molar percentage of As, was found to exhibit a variety of direct bandgaps (from 0.7 eV to 1.35 eV) while still remaining nearly lattice matched to an InP substrate. This was achieved by simultaneously varying both the Ga/In and As/P ratios in the solid solution (Ref 1:49).

Since 1972, GaInAsP has been tested for its usefulness in light-emitting diodes (Refs 9, 10, 11, 38, 49), heterojunction lasers (Refs 19, 20, 21, 50), photoemissive detectors (Refs 12, 23), and microwave devices (Refs 4, 16, 17, 29, 33). The most promising of the many uses proposed for GaInAsP are an optical information transmission system and improved field effect transistors (FETs) and transferred electron devices (TEDs). GaInAsP heterojunction lasers have been built that emit in the 1.1 μm to 1.2 μm region, where fused silica fibers used for optical transmission have minimum loss and dispersion (Ref 38:499). Work by several groups has demonstrated low-field drift mobilities, peak drift velocities and peak/valley ratios in GaInAsP that could lead to the construction of much-improved microwave devices (Refs 16, 29).

Recently, the Air Force Avionics Laboratory has become interested in the remarkable properties of GaInAsP, especially in regards to the construction of improved microwave devices. The construction of such devices requires thin (0.4 μm) epitaxial layers of high purity

and crystalline perfection (Ref 17:1).

Problem Statement

The purpose of this project is to optically characterize undoped layers of GaInAsP grown by liquid phase epitaxy (LPE) on chromium-doped, semi-insulating InP substrates oriented in the [100] and [111] B directions. Specifically, the nature of the light emitted by samples of GaInAsP upon optical excitation will be investigated in an effort to determine what impurity and defect levels are present in the epilayers. The information obtained can be used in further studies to identify impurities and imperfections introduced by the growth process.

The technique chosen for optically characterizing the epitaxial layers of GaInAsP is "photoluminescence." This technique uses light of a certain frequency or narrow range of frequencies to excite electrons in the irradiated material. The light emitted from the sample during its relaxation toward equilibrium is then directed through a spectrometer, which separates the different wavelengths present for analysis. As nearly all the light used to excite the material is absorbed near the surface, this technique cannot be used to profile characteristics as a function of depth without removing layers of material. However, photoluminescence has the advantage of being quick, simple and relatively inexpensive. Sophisticated methods, such as cathodoluminescence, may be employed in later studies to expand on the information obtained here.

II. Theory

Crystal Structure of GaInAsP

Gallium Indium Arsenic Phosphide (GaInAsP) is a quaternary solid solution formed from the Group III elements gallium and indium and the Group V elements arsenic and phosphorous. The crystal structure of GaInAsP can be easily visualized by considering a mixture of the binary III-V compounds GaAs and InP. Both GaAs and InP crystallize in the zinc-blende lattice (Fig. 1). GaInAsP may be visualized as, for example, a GaAs zinc-blende lattice in which a certain amount of the gallium has been replaced by indium in the Group III sublattice and a certain amount of the arsenic has been replaced by phosphorous in the Group V sublattice. This phenomenon

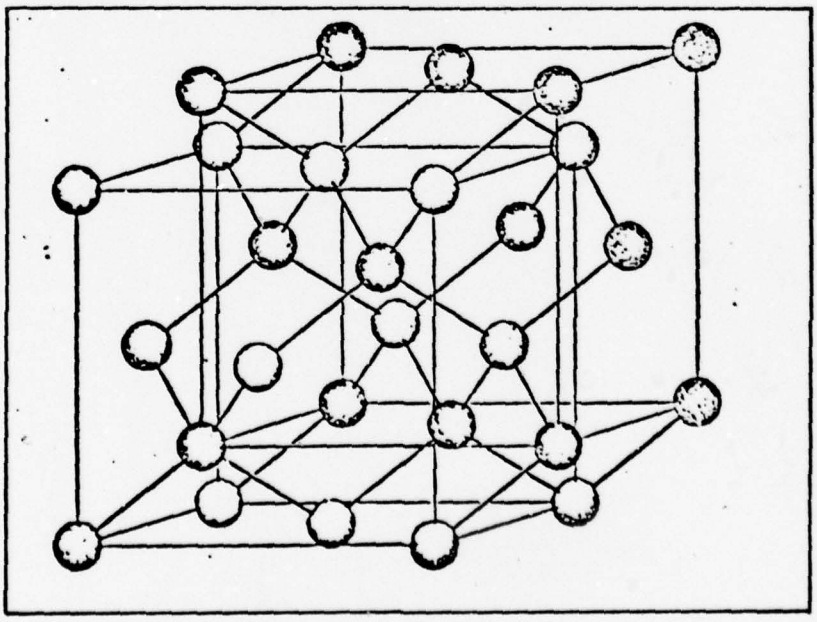

Fig. 1. The zinc-blende lattice, two interpenetrating face-centered cubic lattices (From Ref 30:3)

is called "isovalent substitution," and does not usually result in the formation of impurity levels in solid solutions of III-V compounds (Ref 47:457).

The zinc-blende lattice can be most easily described as two inter-penetrating face-centered cubic (fcc) sublattices (Ref 30:3). The two sublattices are oriented parallel to one another, but are displaced by the lattice vector τ = (a/4, a/4, a/4), where "a" is the edge length of the elementary cube of the fcc lattice. The length of the vector τ is 0.433a. This is also the distance between nearest neighbor atoms (Ref 30:4).

The atoms of the zinc-blende structure have different alignments depending upon the viewing direction through the crystal. These viewing directions may be specified through the use of Miller indices (Ref 25:18). Two such directions are the [111] axis (viewing along the body diagonal of one of the fcc cubic sublattices) and the [110] axis (viewing along a face diagonal of one of the fcc sublattices) (Ref 30:10). These orientations are illustrated in Fig. 2.

If each sublattice of the zinc-blende structure is composed of only one type of atom, a considerable difference in atomic radius can be tolerated between the atoms of each sublattice (for example, in InP the atomic radius mismatch is 30%). When two different elements must be accommodated in each sublattice, as is the case in GaInAsP, then much smaller differences in atomic radius can be tolerated. Quaternary solid solutions of III-V

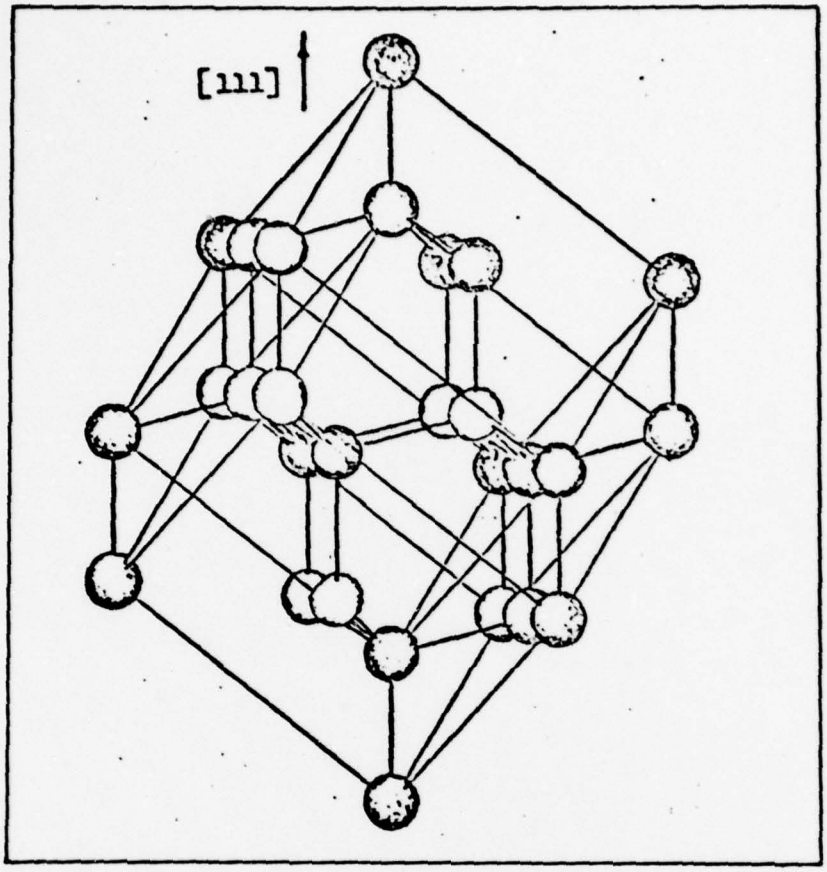

Fig. 2. Zinc-blende lattice, viewed perpendicular to the [11] axis (From Ref 30: 10)

compounds cannot form a single zinc-blende lattice when the atomic radius mismatch exceeds about 17% (Ref 35:1240). Since the atomic radius mismatch of arsenic and phosphorous is 7% and of gallium and indium is 12%, all possible combinations of these four elements can form a single zinc-blende structure (Ref 35:1239).

The sublattice ordering, i.e. the precise positions of the constituent atoms within each sublattice, of GaInAsP has not yet been properly investigated. This is a question of considerable importance, because the state of ordering can influence the electrical (Refs 15, 29) and the thermal

(Ref 16:45-54) properties of a material. A group of researchers led by Dr. J. W. Harrison has recently begun to employ x-ray diffraction techniques to answer this question (Ref 17). To date, Harrison's group has detected modulations of lattice constant in epilayers of GaInAsP grown on InP. It is uncertain whether these modulations arise from compositional fluctuations (sub-lattice disorder) or lattice imperfections (Ref 17:39). Harrison's group is presently engaged in determining the exact degree of short range order present in GaInAsP epilayers grown on InP.

GaInAsP Energy Structure

Ideal Crystals. When a group of atoms are brought together to form a solid such as a crystal, the allowed electronic energy states form bands rather than discrete levels. This band structure at absolute zero consists of a completely filled band (valence band) separated from a higher empty band (conduction band) by a region of forbidden energy states of extent E_G, the band gap (Fig. 3a).

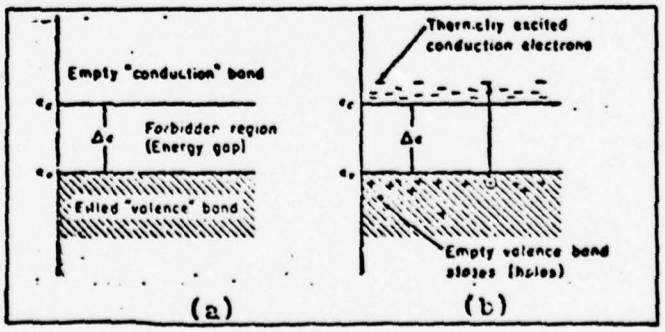

Fig. 3. Conduction and valence bands of a semiconductor at (a) T = 0 (b) T > 0 (From Ref 40:8)

Since a filled band cannot carry a current, solids are perfect insulators at absolute zero. Once the temperature rises above zero, however, there exists a finite probability (which increases with temperature) that some electrons will acquire enough energy to leap the forbidden region and enter the conduction band (CB). These electrons leave behind them empty states in the valence band (VB) that can be mathematically modelled as positively charged particles called "holes" (Fig. 3b). Both the electrons and the holes can acquire a net drift under the influence of an electric field and cause currents to flow in the solid.

It is the extent of the forbidden region and the relative availability of conduction band electrons that determine whether a solid is a metal, a semiconductor, or an insulator. In a semiconductor, the band gap is usually less than three electron volts and the density of electrons in the conduction band is usually less than 10^{20} cm^{-3} (Ref 37:3). Metals have a far larger electron concentration in the conduction band (10^{23} cm^{-3}), and insulators have both a large band gap and a negligible electron concentration in the conduction band.

Real Crystals. When an impurity atom enters an ideal crystal lattice, it introduces additional electronic energy states into the crystal's band structure. If the impurity atom replaces one of the constituent atoms of the crystal, it is called a "substitutional impurity." If the impurity atom occupies one of the spaces between the atoms of the

crystal, it is called an "interstitial impurity." Only substitutional impurities will be discussed here.

When the impurity atom has a higher valence than the atom it has replaced, it is called a "donor" impurity (Ref 25:232). A donor atom provides at least one extra electron to the crystal after it has completed covalent bonding with its neighbors. This extra electron is bound to the donor site in the same fashion an electron is bound to a proton in the familiar hydrogen atom. The only difference is that the atoms of the crystal lattice form a medium of high dielectric constant, K, between the electron and its donor atom. Consequently, the electron's orbital radius is increased by a factor of K, and the usual discrete hydrogenic energy levels are reduced in energy by a factor of K^2 (Ref 7:16). When this extra electron receives enough energy to enter the conduction band, a region of positive charge is left behind. This region forms a donor energy level that falls below the conduction band by an amount equal to the ionization energy of the electron from its donor atom (Fig. 4).

When the impurity atom has a lower valence than the atom it replaces, it is called an "acceptor" (Ref 25:234). The acceptor atom has an unsaturated covalent bond because it has insufficient electrons to bond with all its nearest neighbors. This bond can be saturated by attracting an electron from a nearby atom. In effect, this removes an electron from the valence band. The vacancy left by the electron can be thought of as a positive "hole" circling a negatively charged center. Acceptor atoms form energy

levels that fall above the valence band by an amount E_A, determined by the energy needed to remove an electron from the valence band and attach it to the acceptor atom (Fig. 4).

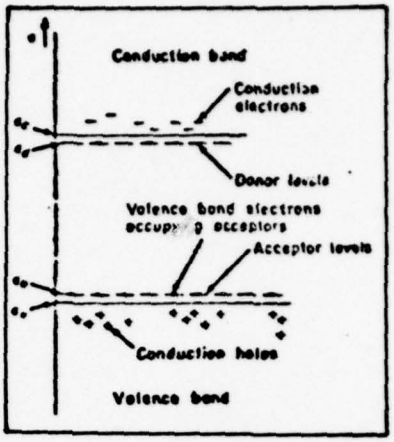

Fig. 4. Energy band structure of a semiconductor, showing donor and acceptor levels (From Ref 40:9)

When the valence of the substitutional impurity is the same as that of the atom it replaces, it may form an "isoelectronic trap" (Ref 45:218). The difference in atomic radius between the isoelectronic impurity and the surrounding atoms introduces a perturbation into the potential field of the host lattice. Provided the mismatch in radius is large enough, this perturbation can trap electrons or holes at the isoelectronic impurity site. The precise trapping mechanism of the isoelectronic impurity site is not well understood. Some examples of isoelectronic traps are bismuth and nitrogen in GaP (Ref 45).

The distance between atoms is not the same in every viewing direction within a crystalline lattice. The banding of electronic energy states will therefore change with the crystallographic direction (Ref 37:3). Although the characteristic energy gap of a semiconductor has the same minimum value in each unit cell of the crystal, its topography within the unit cell can be very complex.

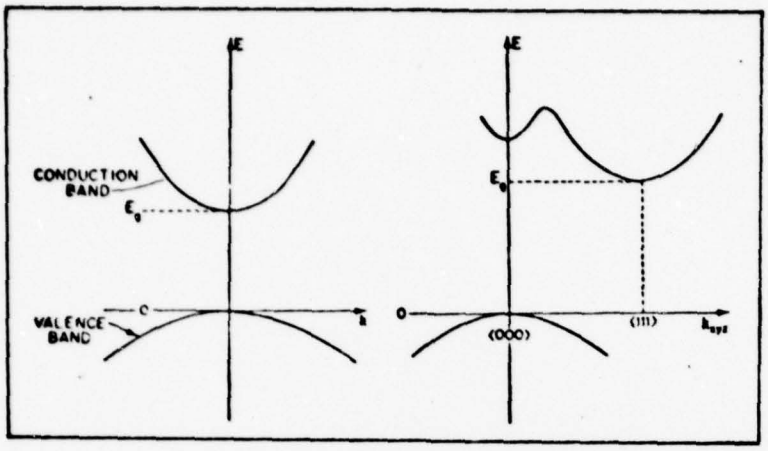

Fig. 5. Energy-momentum diagram in (a) a direct-gap semiconductor, and (b) an indirect-gap semiconductor (From Ref 37: 4,5)

The electronic energy levels in a crystalline lattice are often plotted in energy-momentum space. Since electronic transitions must obey the laws of conservation of energy and momentum, such diagrams are very useful in deciding whether or not a given transition is allowed. Two such energy-momentum diagrams are plotted in Fig. 5. Actually, these diagrams are only two-dimensional sections of a four-dimensional space whose coordinates are energy (E) and three momentum coordinates (k_x, k_y, k_z). Any direction in a crystalline lattice may be specified by picking three values of k_x, k_y, k_z (Ref 37:5). The two general classes of semiconductors are also illustrated in Fig. 5. The direct-gap semiconductor (Fig. 5a) is one in which the lowest minimum of the conduction band and the highest maximum of the valence band both occur at the point (k_x, k_y, k_z) = 0. In the indirect-gap semiconductor,

the highest maximum of the valence band is still at $(k_x, k_y, k_z) = 0$, but the lowest conduction band minimum occurs at some point defining a crystallographic direction (such as [111] in Fig. 5b). An electron cannot transition directly from the lowest conduction band minimum to the highest valence band maximum in an indirect-gap semiconductor without violating the law of conservation of momentum. This transition can only occur with the aid of one or more phonons (quanta of lattice vibrational energy) to conserve momentum.

There are several theoretical or theoretical/empirical methods for determining the energy band structure of semiconducting materials. None of these methods have yet been used on GaInAsP due to the complexity of the problem. GaInAsP is a quaternary material, and such calculations would be far more difficult than for a binary or even a ternary compound. Moreover, every change in the Ga/In or As/P ratios would make a new calculation necessary.

Radiative Transitions

When luminescence is produced as the result of an electron transitioning from a higher energy state to a lower energy state, the transition is called a "radiative" transition. Transitions which do not result in the release of photons are "non-radiative" transitions and include such processes as the Auger effect, surface recombination,

recombination at defects, and phonon emission (Ref 37:161). Significant luminescence generally occurs only when a system is thrown out of equilibrium. This deviation from equilibrium can be produced in a variety of ways, such as by an electron beam (cathodoluminescence) or by optical excitation (photoluminescence) (Ref 37:107-108).

Once electrons have been excited out of the valence band of the semiconductor, there are many paths the electrons can take to return to an equilibrium distribution. Only those transitions which conserve both energy and momentum are allowed. These transitions are illustrated in Fig. 6.

All of the transitions illustrated in Fig. 6 may be assisted by one or more phonons. Phonons exist within all crystalline lattices. The form and precise energies of the phonons depend upon the type of lattice and the nature of the atoms within the lattice. The allowed energies of phonons in the GaInAsP solid solution are not yet known, but can be expected to be on the order of tens of meVs (Ref 46:355).

Excitons. The exciton is basically an electron-hole system. The electron is almost free, but it still feels a slight coulomb attraction to the hole from which it was excited. This attraction causes the electron to remain in orbit around the hole (Ref 7:16). The exciton

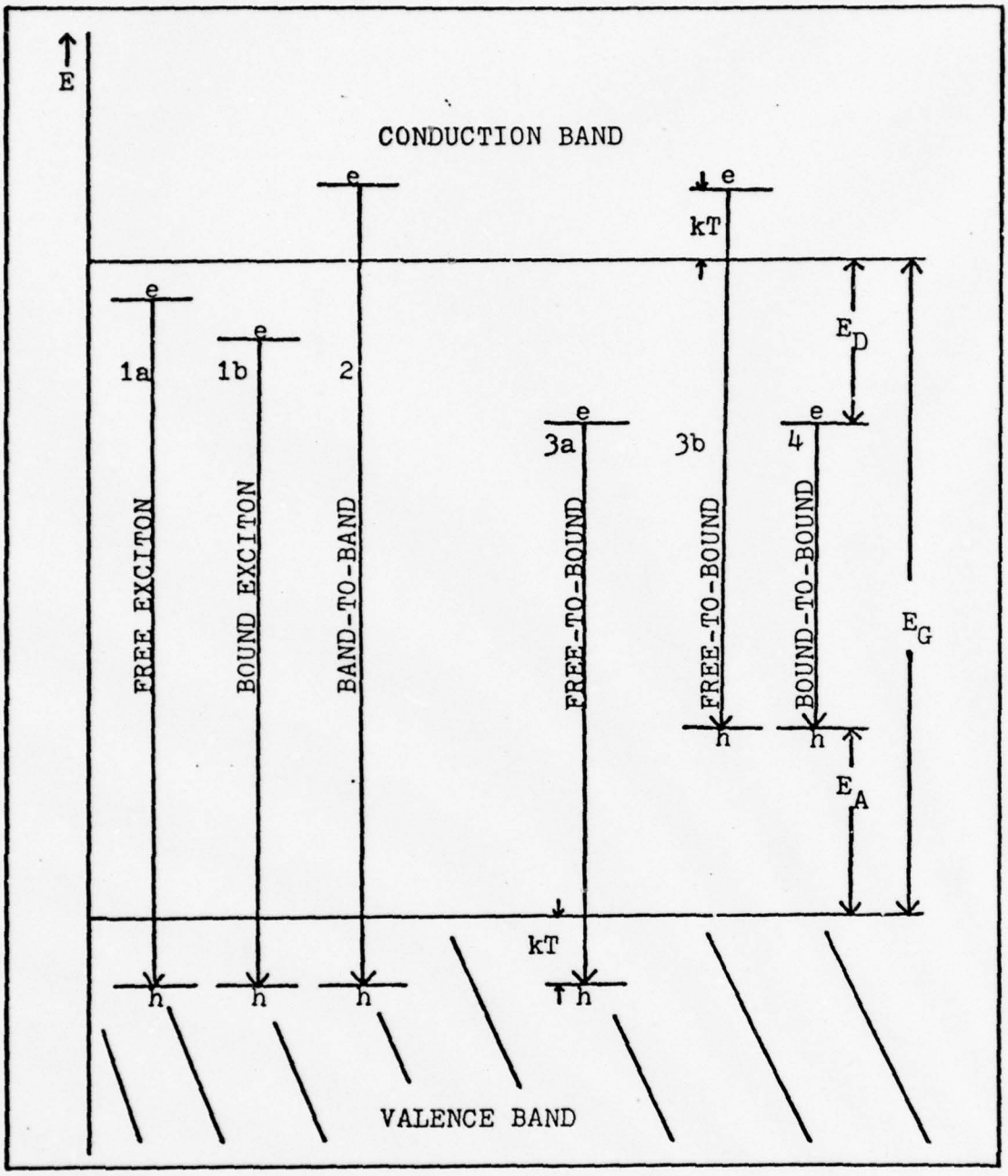

Fig. 6. Allowed Radiative Transitions

resembles a hydrogen atom, but its binding energy is smaller than a hydrogen atom because of the dielectric medium between the hole and the electron. The energy states of the exciton lie just below the conduction band (Fig. 6-1).

The free exciton is composed of a free electron and a free hole (Fig. 6-1a). It can move through the crystal lattice and thus possesses a finite kinetic energy which broadens the exciton levels into bands (Ref 37:114). Free exciton recombination is a very inefficient process, and since free excitons are easily broken up by local fields in impure crystals or by small thermal energies, free exciton recombination is seldom observed (Ref 37:124).

Excitons may become bound in the presence of impurity atoms. When these bound excitons recombine, the emitted radiation is less than that of the free exciton by an amount equal to the binding energy of the exciton to the impurity (Fig. 6-1b) (Ref 7:107). Since bound excitons do not possess the thermal energy of free excitons, bound exciton recombination peaks are characterized by a narrower spectral width (Ref 37:116), generally on the order of one meV. Excitons may be bound to both neutral and ionized donor and acceptor impurities (Ref 37:116-124) and to isoelectronic traps. The exciton bound to a neutral acceptor or donor impurity involves three particles. The three-particle configuration frequently interacts non-radiatively via the Auger effect, which reduces the radiative efficiency of this process.

Band-to-Band. Band-to-band transitions occur when a free electron in the conduction band recombines directly with a free hole in the valence band (Fig. 6-2). A band-to-band emission peak must have a low energy threshold at $h\nu = E_G$, but as the excitation rate or the temperature increases, states deeper in the conduction band become filled. These higher energy electrons may also recombine directly across the band gap, but with a lower transition probability. Band-to-band recombination is therefore characterized by a temperature-dependent high-energy tail and an abrupt low-energy cutoff at E_G (Ref 37:125). Perturbations in this ideal case caused by transitions from the tails of states and impurity bands often change the abrupt low-energy cutoff into a more gradual descent (Ref 37:126).

The change in temperature has additional effects on band-to-band transitions. As the temperature of a semiconductor increases, the bandgap energy invariably decreases. When InP is heated from $78^{\circ}K$ to $300^{\circ}K$, the bandgap energy decreases by about 100 meV (Ref 30:44). The intensity of a band-to-band recombination peak in a direct-gap semiconductor will also decrease with increasing temperature. This is because band-to-band recombination provides the maximum lifetime that a carrier can attain in a semiconductor. Capture into various impurity levels is usually far more rapid, and as the temperature increases carriers migrate more swiftly to impurity sites before

recombination (Ref 46:297). Hall has calculated the functional form of this process. For a direct-gap semiconductor, the intensity of band-to-band recombination is proportional to $T^{-3/2}$ (Ref 26:507). Finally, a band-to-band recombination peak will broaden as temperature increases and the distribution of electrons in the conduction band reaches higher energy states.

A band-to-band recombination peak may then be identified by certain temperature-dependent behavior. First, a band-to-band recombination peak will be asymmetric with a temperature-dependent high-energy tail. The intensity of such a peak will decrease with temperature according to Hall's statistics ($T^{-3/2}$). The half-width (full width at half maximum) of the peak will increase with temperature, and the position of the peak's maximum will shift toward longer wavelengths (lower energies) as the temperature rises.

Free-to-Bound. Free-to-bound transitions occur when a free electron (hole) with an average kinetic energy E_k, primarily temperature dependent, recombines with a trapped hole (electron) localized at an acceptor (donor) impurity site (Fig. 7-3). The energy released when a free hole recombines with an electron trapped at a donor site is (Ref 6:744)

$$E_{fb} = E_G - E_D + E_k + nE_p \qquad (1)$$

The energy released when a free electron recombines with

a hole trapped at an acceptor site is similarly

$$E_{fb} = E_G - E_A + E_k + nE_p \qquad (2)$$

where E_D and E_A are the donor and acceptor energies respectively, E_k is the average kinetic energy of the free carriers, n is the number of phonons (if any) assisting the transition, and E_p is the phonon energy. Since there is some spread of the kinetic energy of the free carriers about the average value E_k, an emission peak due to a free-to-bound emission should be symmetrically displaced about the peak center.

Temperature variation has several effects on a free-to-bound emission peak. As the temperature is increased, the average kinetic energy of the free carriers and the dispersion of kinetic energy about the average also increase. Therefore, the free-to-bound emission peak will broaden as the temperature rises and the position of the peak maximum will shift toward higher energies with respect to the bandgap. Colbow (Ref 6:744) predicts a linear variation of the difference between the no-phonon emission peak and the bandgap energy. Assuming a capture cross-section of free carriers by impurities which is independent of kinetic energy, Colbow arrives at the expression

$$E_k = kT \qquad (3)$$

where k is the familiar Boltzmann constant. In any event, at low temperatures E_k must be small enough so that any

error in equation (3) would be small. In addition, the increased temperature causes thermal detrapping of carriers. This severely reduces the probability of bound exciton, bound-to-bound, and band-to-band transitions. One therefore expects free-to-bound emission peaks to dominate the emission spectrum at higher temperatures ($77^{o}K$) (Ref 39:22).

The free-to-bound emission peak is symmetrically shaped. The position of the peak maximum shifts toward higher energies with respect to the bandgap as the temperature rises, and the peak itself broadens as kT. The free-to-bound peak grows in intensity with respect to bound exciton, bound-to-bound, and band-to-band emission peaks as the temperature rises, leading to dominance at higher temperatures.

Bound-to-Bound. Bound-to-bound transitions occur when an electron trapped at a donor impurity site recombines with a hole trapped at an acceptor impurity site (Fig. 6-4). The emission peaks arising from this type of transition are often called "donor-acceptor pair" peaks because the transitions take place between particular pairs of donor and acceptor impurity sites (Ref 44:67). Provided the donor and acceptor impurities are at a distance large compared to the Bohr radii of the electron at the donor site and the hole at the acceptor site, the transition is given by

$$E_{bb}(r) = E_G - (E_A + E_D) + e^2/\varepsilon r + nE_p \qquad (4)$$

where r is the distance between donor and acceptor, e is

the electronic charge and ϵ is the low frequency dielectric constant of the semiconducting medium (Ref 44:67). The term $e^2/\epsilon r$ represents the coulomb attractive energy between the electron and hole. An additional term of the form $(\alpha/r)^5(e^2/\epsilon r)$ must be added if the donor-acceptor pair is too close (Ref 40:32). This term accounts for van der Waals-like repulsive forces.

If the donor and acceptor atoms occupy lattice sites within the crystal, then they will be located at a set of discrete distances from one another. One expects that these sets of donor-acceptor pairs at discrete distances will give rise to a large number of very sharp peaks in the emission spectrum (Ref 13:285). At larger pair separations (lower energies), the individual peaks become closely spaced due to the r^{-1} coulombic dependence so that the peaks merge into a single broad, featureless band (Ref 44:69). As the pair separation increases, the transition probability must decrease, but the number of available states at a given value of r increases. This statistical distribution of donor-acceptor pair sites determines the precise shape of the broad band.

The temperature dependence of the broad donor-acceptor pair band is very complicated. At first, it was believed that the position of the broad band maximum should increase as the temperature increased (Ref 27:843). The reasoning was that as the temperature increased, carriers on the donor sites (for example) would be thermally released and migrate to more favorable recombination sites. "More

favorable" sites are sites with shorter lifetimes and therefore with smaller separations from an acceptor site. This migration would decrease the average value of the donor-acceptor pair separation, and the position of the donor-acceptor pair band would shift to higher energy with respect to the band edge (Ref 8:792). More recently, Halperin and Zacks developed an expression for the shift of the peak position with temperature (Ref 14). They found that the peak energy should decrease as the temperature increased, reach a minimum at some temperature, then increase upon further warming (Ref 14:2242). Halperin and Zacks dismissed earlier results as a special case occurring only for weak excitations and large average pair separations. These conditions would cause the peak position to reach a minimum at such low temperatures that only the peak shift toward higher energies would be noticeable.

An increase in temperature has a further effect on the donor-acceptor pair band. At low temperatures, when kT is much less than the donor and acceptor binding energies, once a carrier has been trapped it can do nothing but radiate. At higher temperatures, the carriers will spend less time trapped and will be able to migrate to non-radiative recombination centers (Ref 43:A278). This decreases the radiative efficiency of the donor-acceptor pair band which also decreases the intensity of the emission peak.

More readily identifiable changes occur when the excitation energy is varied. The probability of recombination is dependent on the square of the overlap of the hole and electron wave functions (Ref 39:25). The probability of recombination will therefore be greatest for those pairs with the smallest separation. As the intensity of excitation increases, the pairs with large separations will become saturated because of their low transition probabilities (Ref 43:A278). The majority of the recombination will then take place between closer pairs, since they have the shortest lifetimes (Ref 8:791). These close pairs have higher coulombic energies than the far pairs, so the broad peak will shift toward higher energies. Naturally, a decrease in excitation intensity will have the opposite effect.

A change in the impurity concentration of a semiconductor can have a similar effect on the donor-acceptor pair band. With decreasing impurity concentration, the average donor-acceptor separation increases and the position of the peak shifts to lower energies (Ref 5:1000). Associated with this shift to lower energies is a decrease in intensity of the donor-acceptor pair emission peak. If there are fewer impurity atoms in the crystal operating as recombination sites, there will be less luminescence produced.

We have seen that the bound-to-bound emission peak has certain definite patterns of behavior. The position of the emission peak will at first shift to lower energies as temperature increases, then reach a minimum, and shift

towards higher energies with further warming. The intensity of the emission peak will decrease as thermal detrapping releases carriers from the donor and/or acceptor recombination sites. An increase in the excitation intensity shifts the position of the emission peak toward higher energies, as will an increase in the impurity concentration. However, the series of discrete lines resulting from nearest-neighbor pairs is the most definite "signature" of bound-to-bound emission. Unfortunately, it is often very difficult to see these sharp lines. All experimental equipment has limited resolution, but even with the finest resolution available it is often impossible to see the sharp lines. If the donor impurity level lies very close to the bottom of the conduction band, it is likely that the coulombic energy term will raise the energy of the discrete lines above the bandgap energy. If this happens, the luminescence from the near pairs will be "self-absorbed" by the crystal and will not reach the observer (Ref 37:127).

III. Experiment

The GaInAsP sample under investigation was contained in the innermost chamber of a cryogenic dewar and excited by the light from an argon-ion laser. The sample luminescence induced by the laser was collected by a system of lenses, chopped by a mechanical chopper, and then focussed on the entrance slit of a spectrometer. The light dispersed by the spectrometer was detected by a cooled PbS photoconductor and compared to a reference signal from the mechanical chopper by a lock-in amplifier. The output of the lock-in amplifier was displayed on an X-Y recorder. The equipment used in this experiment is diagrammed in Fig. 7.

Equipment

Sample Environment. The sample environment was provided by a Janis Detachable-Tail Research dewar. The dewar consisted of three concentric cylinders, each separated from the others by vacuum walls. The sample chamber was the innermost cylinder of the dewar. It was located in the tail of the dewar, which extended below the level of the two remaining cylinders. The outer cylinder was used as a liquid nitrogen reservoir, and the middle cylinder contained liquid helium.

The sample was mounted on a two and three-quarters inch long copper block at the end of a three foot stainless steel rod. The top of the sample rod consisted of a metal assembly which provided electrical connections to the copper

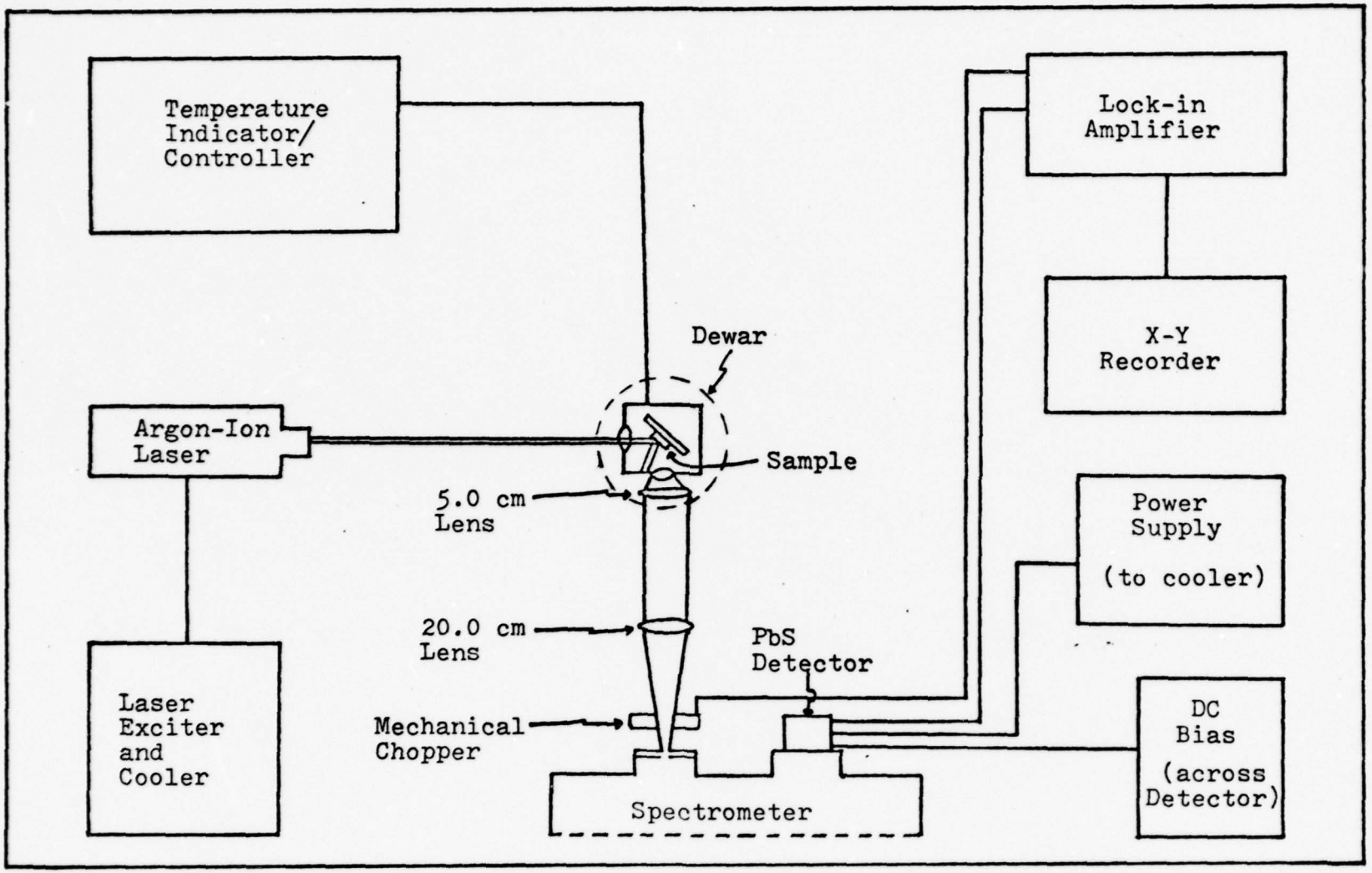

Fig. 7. Block Diagram of Experimental Apparatus

block via insulated wires wrapped around the steel rod. The top of the sample rod was sealed to the dewar with an O-ring. Three resistive heaters were embedded in the top of the sample block, and a GaAs temperature-sensing diode was mounted with RTV silicone behind and a quarter of an inch below the sample mounting area. When the sample was lowered into the sample chamber on the steel rod, the sample was observed from outside through three quartz windows set in the dewar's tail.

A Welch Scientific #1397 mechanical vacuum pump was used to evacuate the dewar's insulating walls and to clear the sample chamber and the innermost of the cryogenic-fluid chambers of moisture. The vacuum was measured at two points by calibrated thermocouple vacuum gauges accurate to one micron.

The resistive heaters were controlled by a Cryotronics Model DTC-500 Temperature Indicator/Controller. This device compared the voltage across the temperature-sensing GaAs diode to a voltage set externally at the controller (the set-point voltage). When the diode voltage rose above the set-point voltage, indicating a drop in temperature, the controller supplied current to the heaters that was proportional to the difference between the set-point and diode voltages. The proportionality factor could be altered by a dial on the controller's panel.

A capillary tube connected the inner cryogenic cylinder, which was the liquid helium reservoir, to the bottom of the

sample chamber. A gas-relief valve on the outside of the dewar could be used in conjunction with a valve controlling the capillary tube to regulate the flow of liquid helium between the cryogenic cylinder and the sample chamber. With experience, the flow of liquid helium could be varied from the point of flooding the sample chamber with liquid to maintaining a small, steady flow of cold helium gas past the sample block. The temperature of the sample block was determined by reading the voltage across the GaAs diode. This voltage was read with the temperature controller. When the set-point voltage was within 0.1 mV of the diode voltage, a sensitive null meter on the face of the temperature controller zeroed. This provided an accuracy of better than 0.1°K in reading the sample block temperature.

Sample Excitation. The sample was optically excited with a water-cooled Spectra Physics Model 164 argon-ion laser and Model 265 Exciter. The laser provided a number of emission lines ranging from 4579 Å to 5145 Å in wavelength. Power output ranged from 150 mW on the 4579 Å line to 800 mW on the 5145 Å line. Output power was read from the exciter's control panel. No lenses or filters were placed between the laser and the quartz entrance window of the sample chamber to alter the beam's characteristics.

Emission Analysis. Sample luminescence left the sample chamber by means of a quartz window at right angles to the entrance window. The luminescence was collected by a large (2 inch diameter) biconvex glass lens with a focal length of

5.0 cm, and focussed onto the entrance slit of a spectrometer by a 20.0 cm glass lens. The luminescence was chopped at either 225 hz or 690 hz at the entrance slit of the spectrometer by a mechanical chopper.

The spectrometer used was a Jarrell-Ash Model 82-020 (f/8.6, 0.5 meter, Ebert mounting) with Model 82-093 curved slit assembly and an optional 590 grooves per mm diffraction grating. The spectrometer's electric, sine-bar scanning drive provided eight speeds varying from 4 Å/min to 1000 Å/min when used with the optional grating. The optical range of the spectrometer was 3800 Å to 18,200 Å in the first order. Both factory test data and a series of calibration runs indicated a scanning accuracy better than 2 Å between 8000 Å and 14,000 Å. At the speeds used to obtain data, the resolution of the spectrometer ranged from 7 Å to less than 5 Å (depending upon the slit width).

The dispersed light at the exit slit was detected by an IR Industries Model TO-2667 PbS detector thermoelectrically cooled to -20°C. Power for the single-stage cooler was provided by a Power/Mate Corporation power supply supplying 1.5 A and 1.0 V with less than 10% ripple. The spectral response of the PbS photoconductor ranged from 58% at 10,000 Å to 90% at 20,000 Å (Fig. 8). The detectivity of the detector varied slightly with the chopping frequency (Fig. 9). The detector used in this experiment had a peak D^* of 1.38×10^{11} cm$\sqrt{\text{hz}}$/W (500°K, 750 hz, 1 hz). No

corrections were made to the recorded spectra for either the spectral or the frequency response of the detector. The detector was biased at 70 V by a pair of dry-cell batteries.

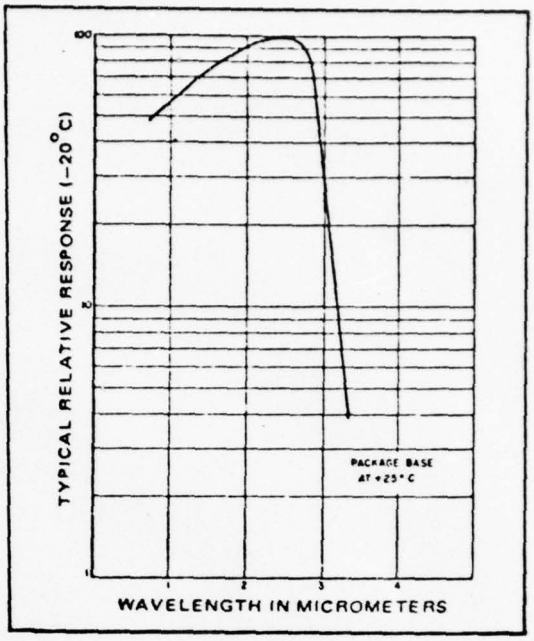

Fig. 8. Spectral response of a PbS photoconductor (From Ref 51)

Recording System. The signal from the PbS detector was sent to a Keithley Model 840 Autoloc Amplifier where it was compared to a reference signal produced by a magnetic transducer in the mechanical chopper. The use of phase-lock techniques has the advantage of eliminating all noise not precisely in phase with the reference signal. The filtered signal was then amplified in the Keithley Model 840 and used as the Y-input of a Houston Instruments Omnigraphic 2000 X-Y Recorder. The X-axis of the recorder was driven internally on a time base, which was always set at 5 sec/cm.

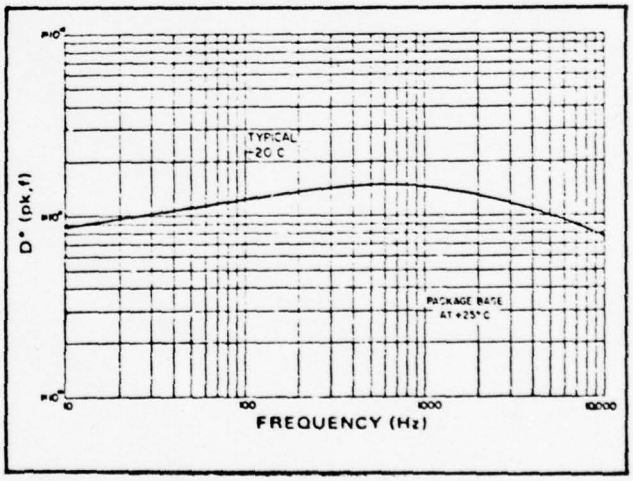

Fig. 9. Frequency response of a PbS photoconductor (From Ref 51)

Experimental Procedure

Sample Mounting. The sample under investigation was mounted to the surface of the copper sample block behind a thin copper mask. A thin film of InGaSn was placed on the back of the sample to improve thermal contact between the sample and the copper block. Two small screws held the copper mask to the sample block and provided a gentle pressure that held the sample firmly to the surface of the block. A 1/8 in diameter hole in the copper mask exposed the sample's surface to excitation by the argon-ion laser.

System Alignment. Both the laser and the spectrometer were placed on wooden mounts designed to keep the laser's bore and the spectrometer's slits level and at an equal height above the laboratory floor. The sample dewar was fixed to an elevating table and raised until the laser beam struck the face of the sample in the dewar. The sample was rotated so that the reflection of the laser beam struck the closed entrance slit of the spectrometer. The dewar and laser were then moved until the reflected beam shined on the exact center of the slit. The first lens (focal length of 5.0 cm) was placed near the exit window of the sample chamber and moved vertically and horizontally until the reflected beam passed through the center, once more shining on the entrance slit of the spectrometer. The second lens (focal length of 20.0 cm) was placed about a focal length from the entrance slit of the spectrometer and the same alignment procedure followed as for the first

lens.

Leaving the entrance slit closed, the top of the spectrometer was opened and a white card placed between the grating and the mirror. The entrance slit was then opened and the position of the laser beam noted on the card. The spectrometer was moved until the beam was imaged in the center of the grating. A thin piece of tissue was placed just inside the entrance slit and the height of the beam above the spectrometer's base was checked simultaneously at the entrance slit and the grating. The sample was then rotated until the specular reflection of the laser beam was just confined to the sample chamber. An image of the surface of the sample was still visible at the spectrometer in scattered laser light. Both lenses were moved along the line between the spectrometer and the sample chamber until this image was brought into a sharp focus. Finally, the mechanical chopper was positioned just in front of the entrance slit.

Data Collection. Once the initial alignment was complete, the capillary valve was opened until positive pressure was felt at the sample chamber gas-relief valve. This insured that moisture-laden air could not enter the sample chamber. The gas-relief valve was opened, and the capillary valve was set to flood the sample chamber with liquid helium. The liquid helium level was maintained above the level of the sample.

The spectrometer was manually scanned until luminescence

was observed. Setting the spectrometer on a luminescence peak, the signal entering the lock-in amplifier was then phase-locked to the reference signal so that only that part of the signal in phase with the reference was amplified. The lenses were slowly moved independently in all three directions until the luminescence entering the spectrometer was maximized. The 4.2°K spectra were then taken.

To raise the temperature of the sample, the gas-relief valve was closed. Back pressure quickly built up in the sample chamber that forced the liquid helium back into the inner cryogenic liquid reservoir. The gas-relief valve was then slowly opened to allow a stream of cold gas to pass across the sample block. This stream of cold gas, in conjunction with the three heaters at the top of the sample block, was used to regulate the temperature of the sample block between 6.6°K and 100°K. This temperature regulation was accomplished by the temperature controller, which sent a regulated current through the heaters until the temperature of the sample block matched a pre-set temperature. Experience showed that the temperature could be easily controlled to within $\pm$0.2°K in this fashion.

When it was necessary to raise the temperature to a new value, the set-point dial on the temperature controller was set at a voltage which corresponded to the new temperature. The gas-relief valve was closed until the heaters had raised the temperature of the sample block to within -1.0°K of the desired temperature. Then the gas-relief

valve was opened until the flow of cold gas could prevent the temperature of the sample block from rising above the desired temperature.

It is emphasized that the temperature controller could only control the sample block temperature. The GaAs diode could not be set to read directly the sample temperature, and the sample was probably slightly warmer due to laser heating. The exact degree of thermal contact was unknown, although a layer of InGaSn was used between the block and the sample to improve matters.

Spectra were typically taken at 4.2°K, 6.6°K, 10°K, and then at 10°K increments beyond that to either 90°K or 100°K. The first spectrum at each temperature was taken with the spectrometer slits at 400 μm, the full-open position. This provided a resolution better than 8 Å, which corresponds to approximately 1.0 meV in the wavelength region between 10,000 Å and 13,000 Å. The scanning speed was 250 Å/min. If fine structure was suspected, further spectra were taken with slit widths of 270 μm(resolution of 7 Å), 150 μm(resolution of 6 Å), or 75 μm(resolution of 5 Å) at a scanning speed of either 100 Å/min or 40 Å/min. In all cases, the spectral region beyond the structure observed at 6.6°K was scanned out to 16,000 Å at the highest amplifier sensitivity possible in search of further emission peaks.

Samples QF 3003, Q 2945/106, and 6-1A were excited with the 4880 Å (700 mW) laser line. Sample Q 2601-0

was excited with the 4765 Å (300 mW) laser line since the second order of the 4880 Å laser line interfered with the sample's emission spectrum.

Sample Information

Liquid phase epitaxy (LPE) is the process by which a thin single-crystal film is grown from a dilute molten solution on a flat, oriented, single-crystal substrate (Ref 31:184). The specimens investigated in this report were grown at Varian Associates by constant-temperature LPE in a horizontal growth system with an acid-cleaned graphite boat and multiple-bin slide (Ref 33:1). The LPE layers were grown on chromium-doped, semi-insulating [100]- or [111]B-oriented InP substrates. The GaInAsP quaternary melts consisted of 6-9's pure In and high-purity InP, GaAs, and InAs. The precise liquidus composition of each melt was determined from thermodynamic data and empirically adjusted to achieve a good lattice match to the InP substrate (Ref 33:1). The melt was heated at 650°C in a leak-tight quartz furnace tube by a roll-on furnace (Ref 4:C2). Cooling was accomplished by a mechanical programmer capable of various cooling rates.

The growth reactor was purged with pure hydrogen gas for one hour to eliminate oxygen contamination in the gas stream (Ref 33:1). A protective InP cover wafer was placed on top of the substrate during warm-up to prevent surface degradation through thermal P loss. If the surface was especially damaged, a pure In etch melt was used to remove the damaged surface prior to epitaxial growth (Ref 33:2).

Hall-van der Pauw measurements were used to determine the carrier concentration and mobility of each of the samples at room temperature and 77°K. Epilayer thickness was determined by the growth time (Ref 33:1), and the room temperature bandgap was estimated by extrapolating photoluminescent measurements at 77°K to room temperature. All of this information is listed in Table I, and was made available by Varian Associates of California.

The indium used in the preparation of sample Q 2601-0 was Johnson and Matthey grade A1A. This particular grade of indium has a very low silicon content and has yielded many epilayers of high purity. It is believed that sample Q 2945/106 was unintentionally contaminated with sulfur (Ref 34). It is the oldest of the samples (over one year old), and growth methods at Varian were not well-developed at the time of its preparation.

Table I. Information Concerning the GaInAsP Samples								
Sample #	$n \times 10^{16}$ (cm^{-3})		μ (cm^2/V-sec)		E_G (eV)	d (μm)	Substrate Orientation	In Source
	300°K	77°K	300°K	77°K				
Q2601-0	1.7	1.4	3507	10,590	1.2	1	[100]	J & M A1A
QF 3003	3.7	3.1	2771	5270	1.15	1.5	[100]	MCP
Q2945/ 106	51.0	47.0	2749	5179	1.05	0.7	[111] B	?

(n = carrier concentration, μ = mobility, E_G = room temperature bandgap, d = epilayer thickness)

(Data supplied by Varian Associates.)

IV. Results and Discussion

The emission spectra of the three GaInAsP samples are similar. Each consists of a relatively narrow, near-band edge peak followed by a broader peak at longer wavelength. In interpreting the shifts of the peaks in GaInAsP with temperature a vital piece of information is missing. We do not know how the bandgap energy changes with temperature. However, the bandgap of a semiconductor generally decreases with increasing temperature, so that we know the general behavior of the bandgap (Ref 6:748).

The emission spectrum of the LPE InP on InP sample (6-1A) was taken to test the resolution of the experimental system and as an example of a perfectly lattice matched case. Its emission spectrum consists of a narrow peak with a low energy shoulder near the band edge, a broader peak at longer wavelength, and a very small peak which is 43 meV below the broad peak at all temperatures.

Temperature Dependence

Sample Q 2945/106. At 6.6°K, the emission spectrum of sample Q 2945/106 is dominated by two peaks 15 meV apart (Fig. 10). The smaller peak (A) is centered at 1.072 eV; the larger peak (B) is centered at 1.057 eV. Peak A is the narrower peak, with a half-width (full width at half maximum) of 17.7 meV. Peak B is approximately 30 meV wide.

Between 10°K and 30°K, peak B moves toward longer wavelength and becomes smaller with respect to peak A. By 30°K, peak A is at 1.073 eV. Peak B is located at 1.050 eV and is

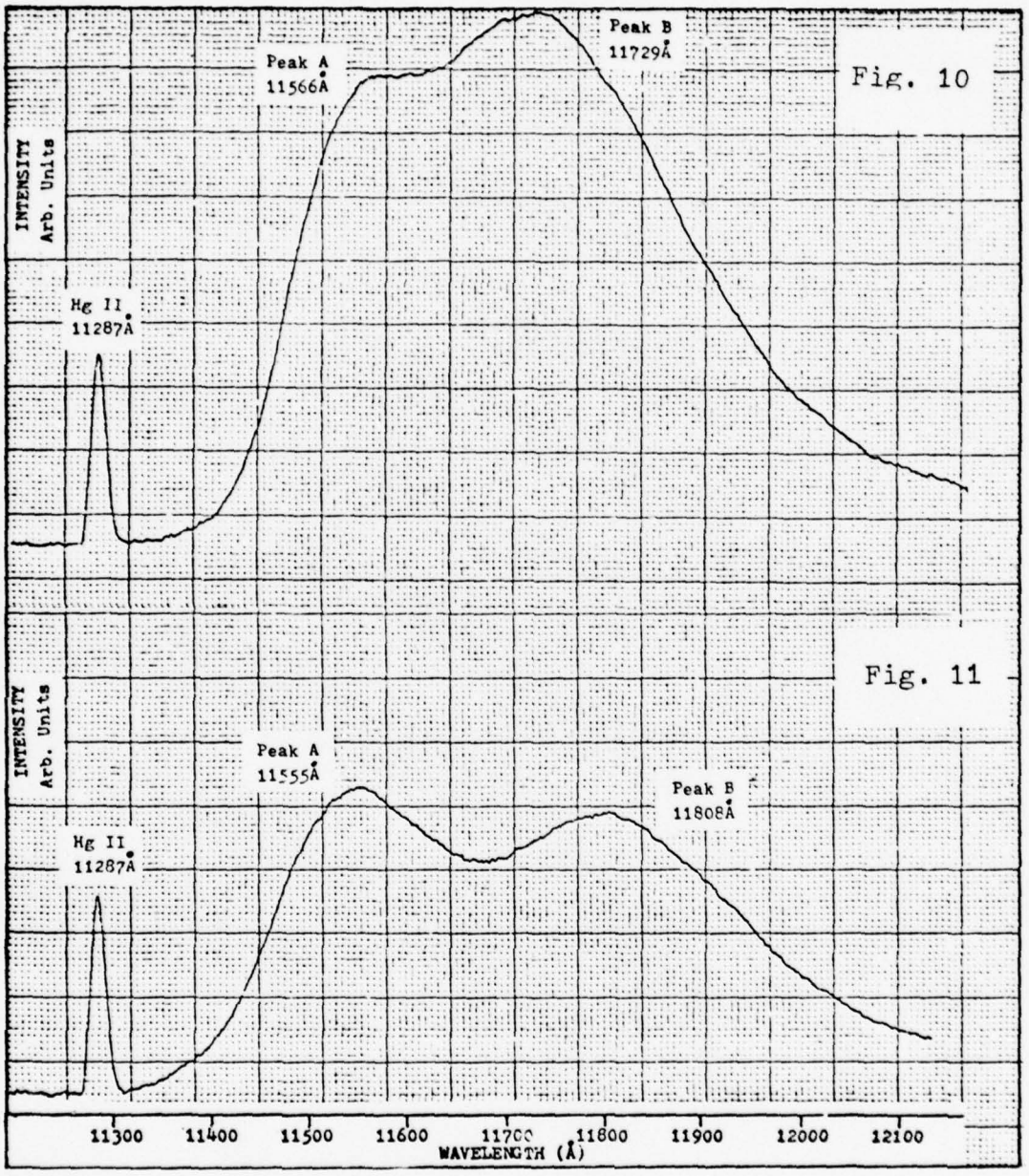

Fig. 10. Q 2945/106 at 6.6°K

Fig. 11. Q 2945/106 at 30°K

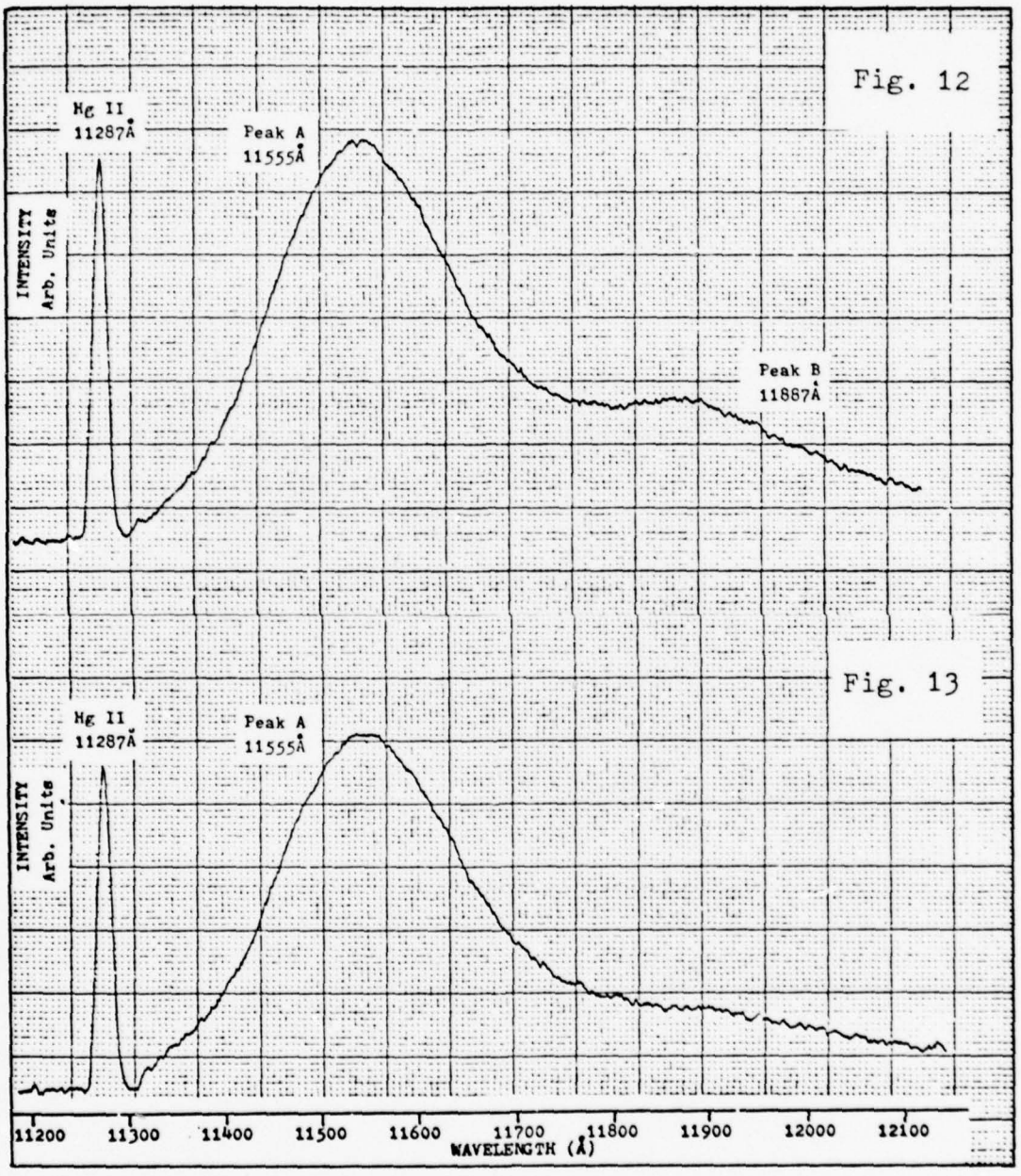

Fig. 12. Q 2945/106 at 45°K

Fig. 13. Q 2945/106 at 50°K

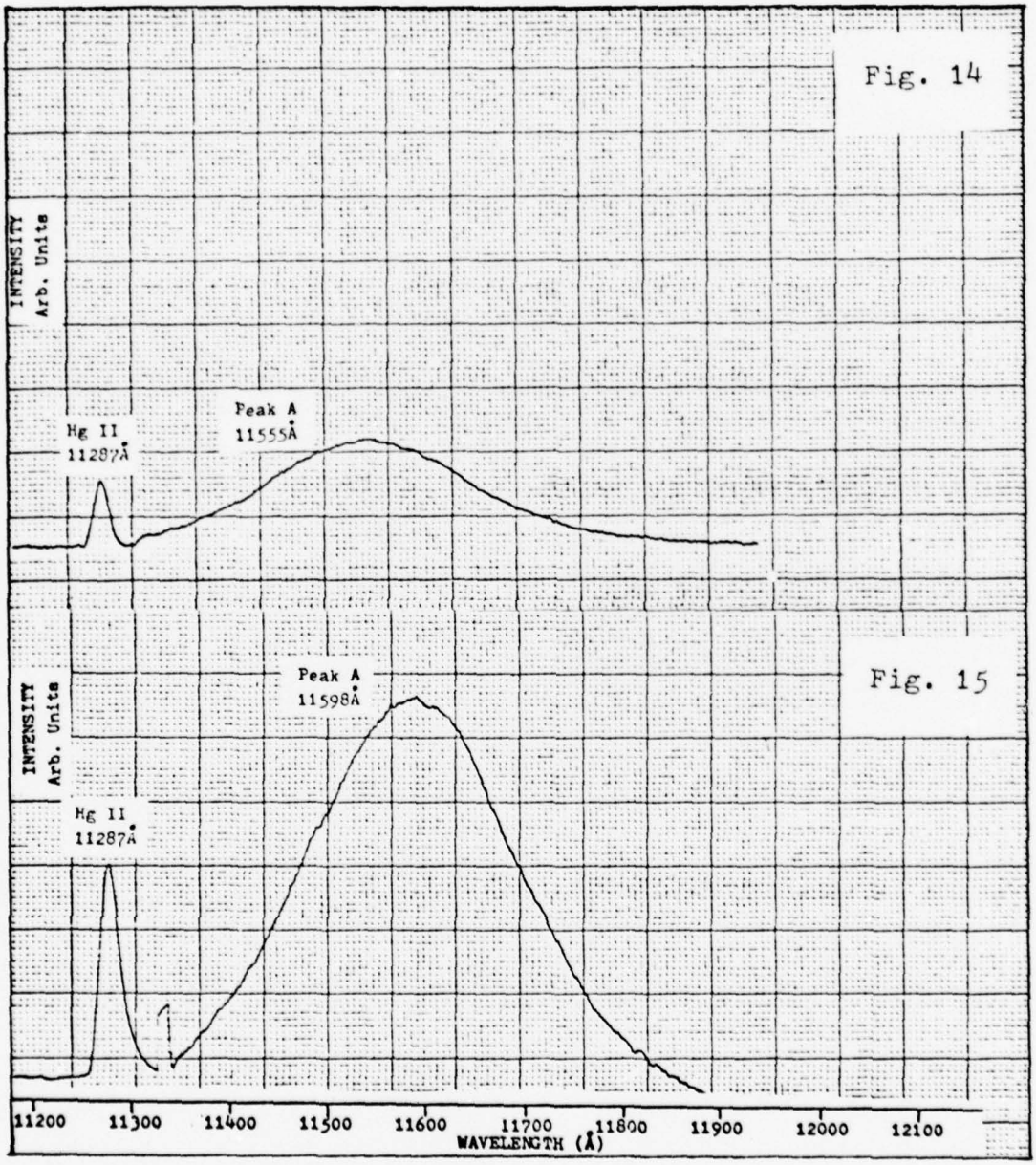

Fig. 14. Q 2945/106 at 70°K

Fig. 15. Q 2945/106 at 90°K

now smaller than peak A (Fig. 11). Neither peak has grown much wider.

At 45°K, peak A is still at 1.073 eV, but it is now 20 meV wide (Fig. 12). Peak B is visible, but only a third as large as peak A. Peak B has shifted to 1.043 eV and has not widened perceptibly. Five degrees later, at 50°K, peak B is no more than a prolonged low energy tail on peak A (Fig. 13).

Between 50°K and 70°K, peak A continues to diminish slowly in size and grow wider, but it does not shift its location. At 70°K, peak A is 25 meV wide (Fig. 14), and peak B has disappeared.

Peak A begins to shift toward longer wavelength at about 75°K. When the temperature has reached 90°K, the maximum of peak A is at 1.069 eV, a peak shift of 5 meV. The peak is now 26 meV wide (Fig. 15).

The temperature dependences of peak location, peak height and half-width are illustrated graphically in Figs. 16, 17, and 18 respectively. The sudden jump in the peak height of peak A indicated at 70°K in Fig. 17 is the result of data taken on different days under slightly different conditions.

The position of peak A with respect to the probable band edge suggests that it is the result of exciton, band-to-band or free-to-bound recombination. However, this peak is too wide and quenches far too slowly to be due to exciton recombination. Peak A is also symmetrical; it has no temperature-dependent high-energy tail such as would be

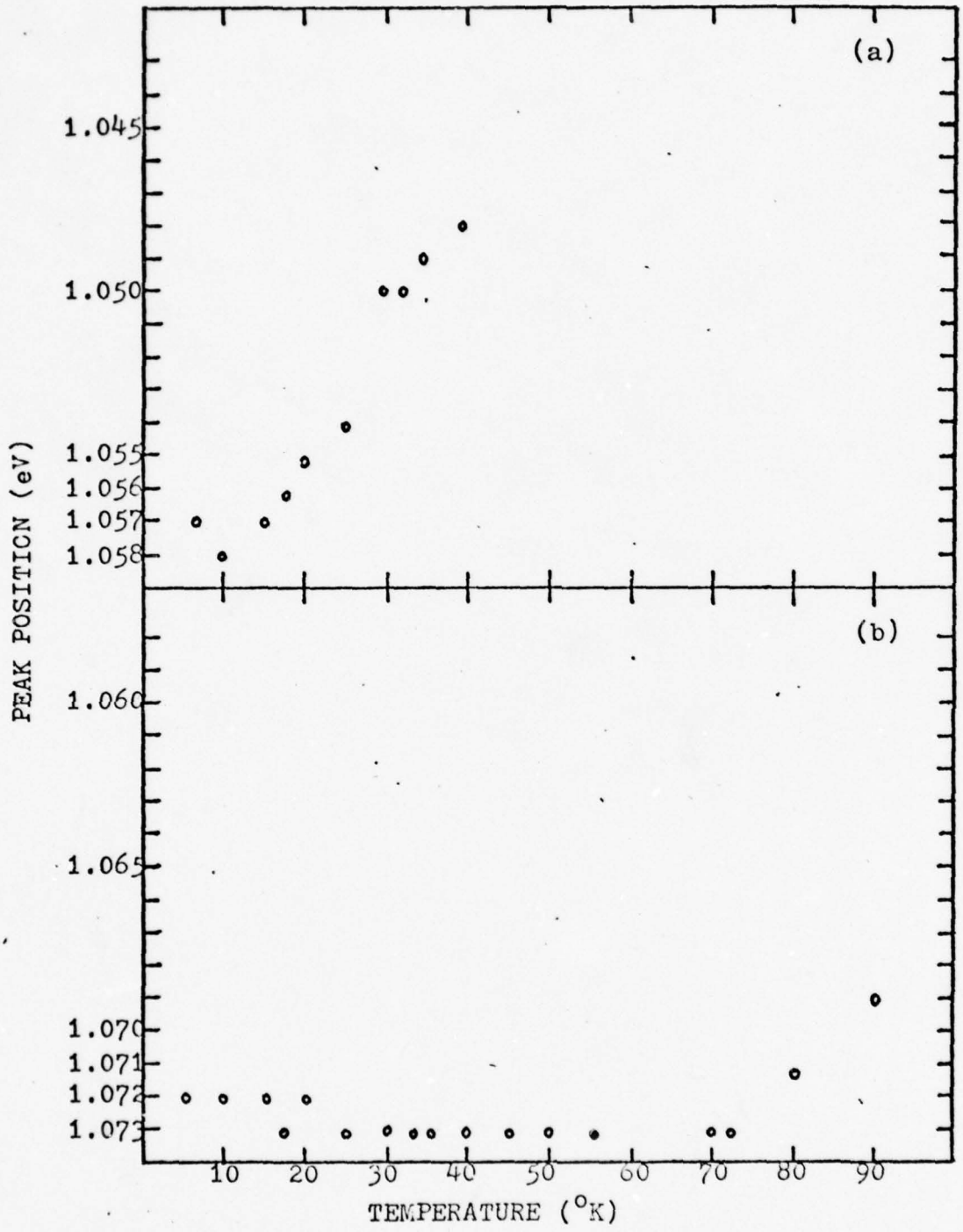

Fig. 16. Q 2945/106: Peak position as a function of temperature for peak B (a) and peak A (b)

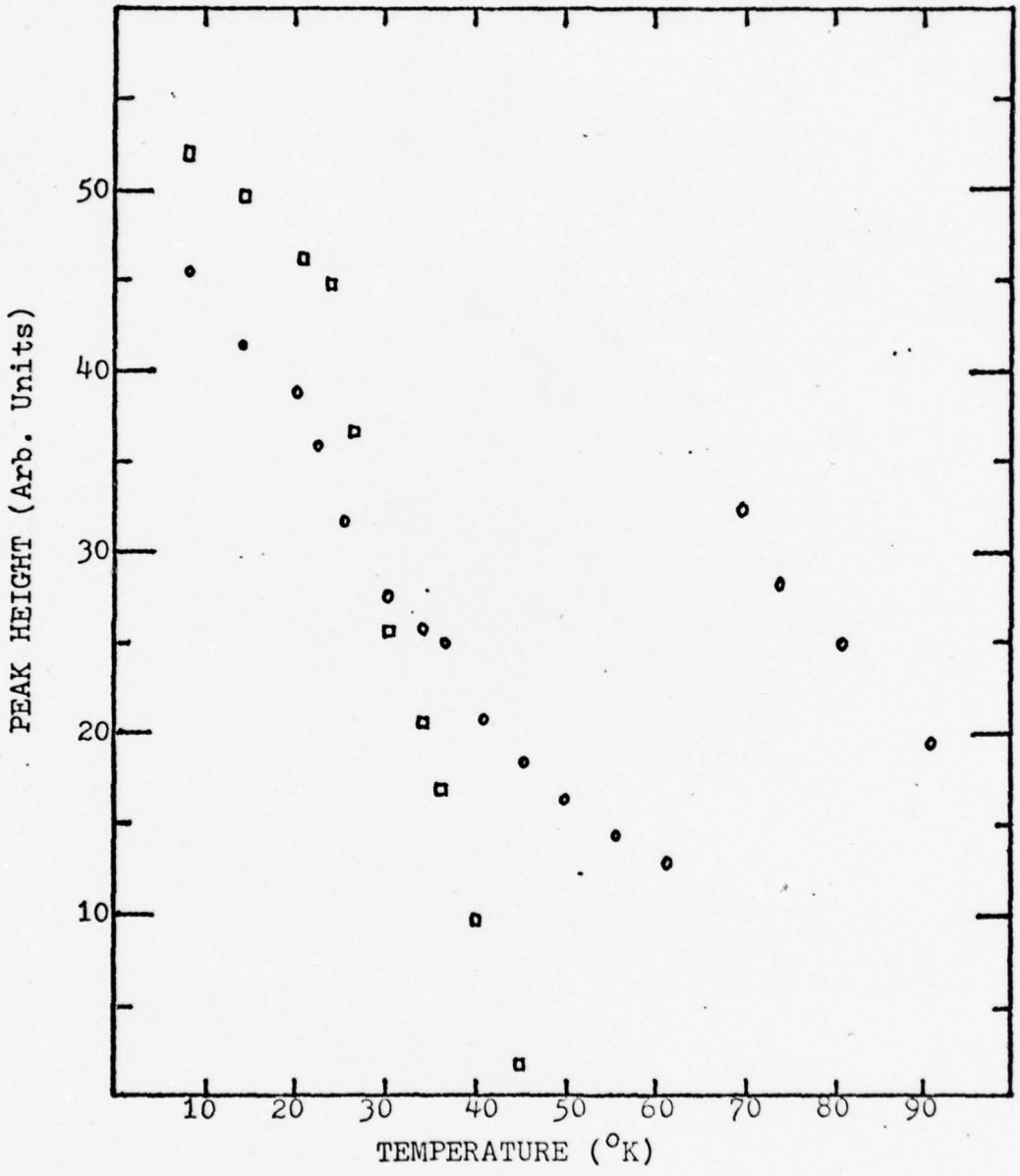

Fig. 17. Q 2945/106: Variation of peak height with temperature for peak A (o) and peak B (□)

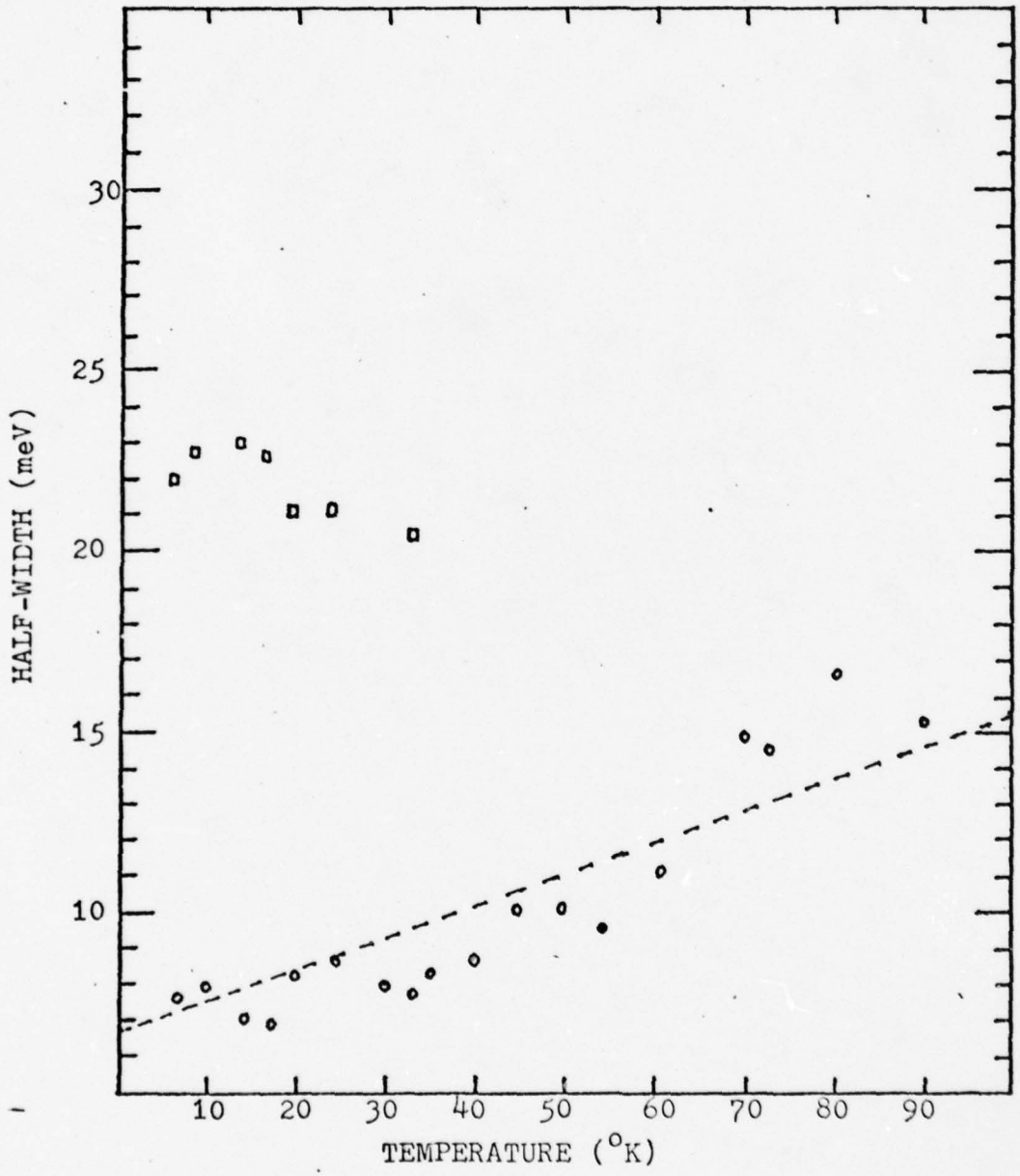

Fig. 18. Q 2945/106: Variation of half-width (full width at half maximum) with temperature for peak A (o) and peak B (□). The dotted line has a slope equal to "k", the Boltzmann constant

expected in a band-to-band recombination peak. Band-to-band recombination radiation is also a strong function of temperature and would probably vanish from the emission spectrum long before the temperature reached 90°K.

If it is assumed that the bandgap of GaInAsP varies with temperature in a manner similar to the bandgap of GaAs, then

$$E_G(T) = E_G(0) - aT^2/(B + T) \qquad (5)$$

where $E_G(0)$ is the value of the bandgap at absolute zero (not known), T is the temperature in degrees Kelvin, a = 8.87×10^{-4}, and B = 572 (Ref 37:27). Comparing the shift of peak A with temperature (Fig. 16b) to this expression for $E_G(T)$, it is found that peak A shifts linearly toward higher energy with respect to $E_G(0)$ as the temperature rises. This linear shift with respect to the bandgap as the temperature rises is characteristic of free-to-bound recombination. Peak A also widens according to kT, which is typical of a free-to-bound recombination peak (Fig. 18).

The position of peak B with respect to peak A suggests that it is the result of donor-acceptor pair recombination. Peak B does quench swiftly with rising temperature, as a donor-acceptor pair recombination peak should (Fig. 17). Additionally, peak B quickly shifts toward longer wavelengths as the temperature rises (Fig. 16a). If peak B showed signs of reversing the direction of its peak shift, the test of Halperin and Zacks (Ref 14) would confirm that it was the result of donor-acceptor pair recombination.

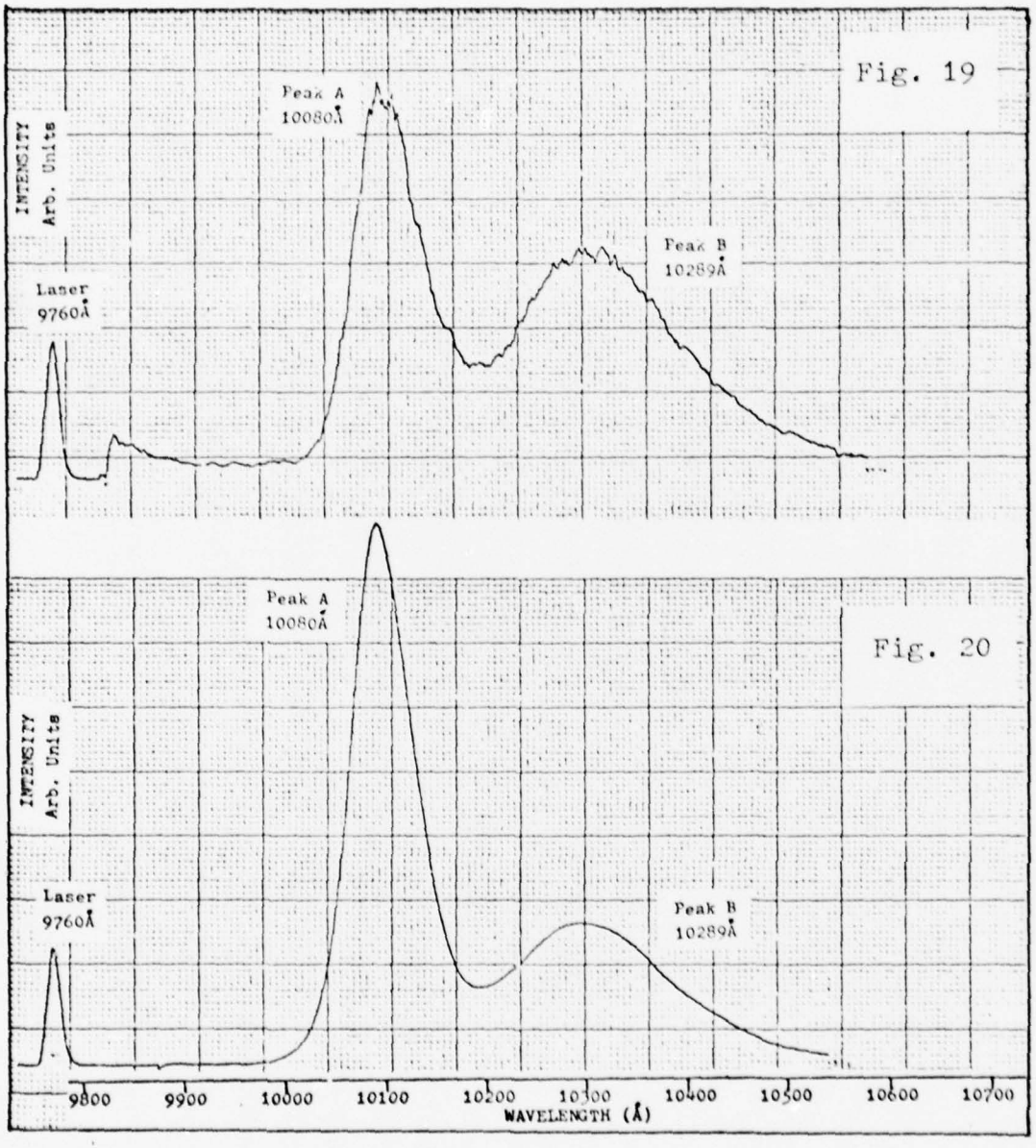

Fig. 19. QF 3003 at 4.2°K

Fig. 20. QF 3003 at 10°K

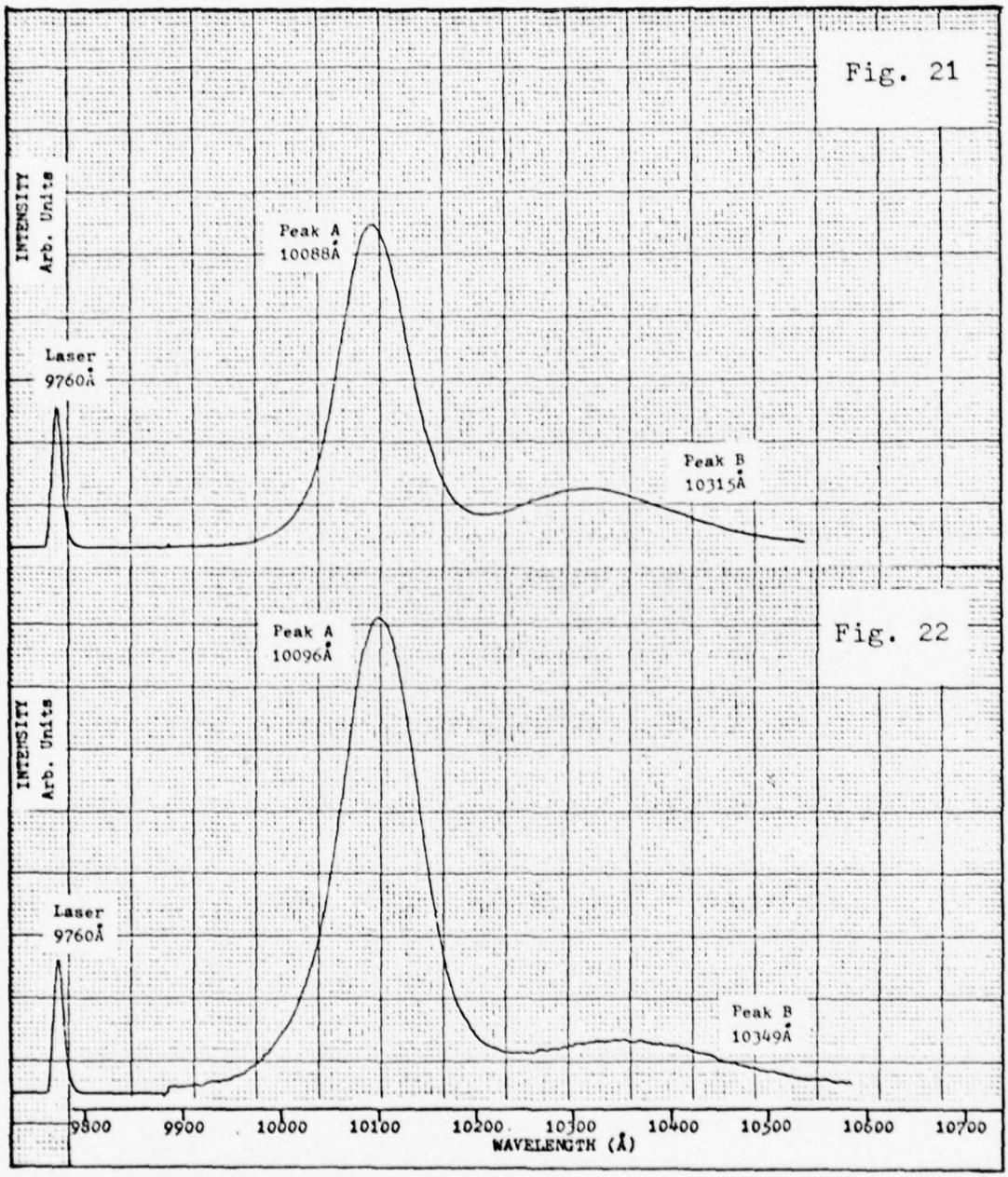

Fig. 21. QF 3003 at 28°K

Fig. 22. QF 3003 at 45°K

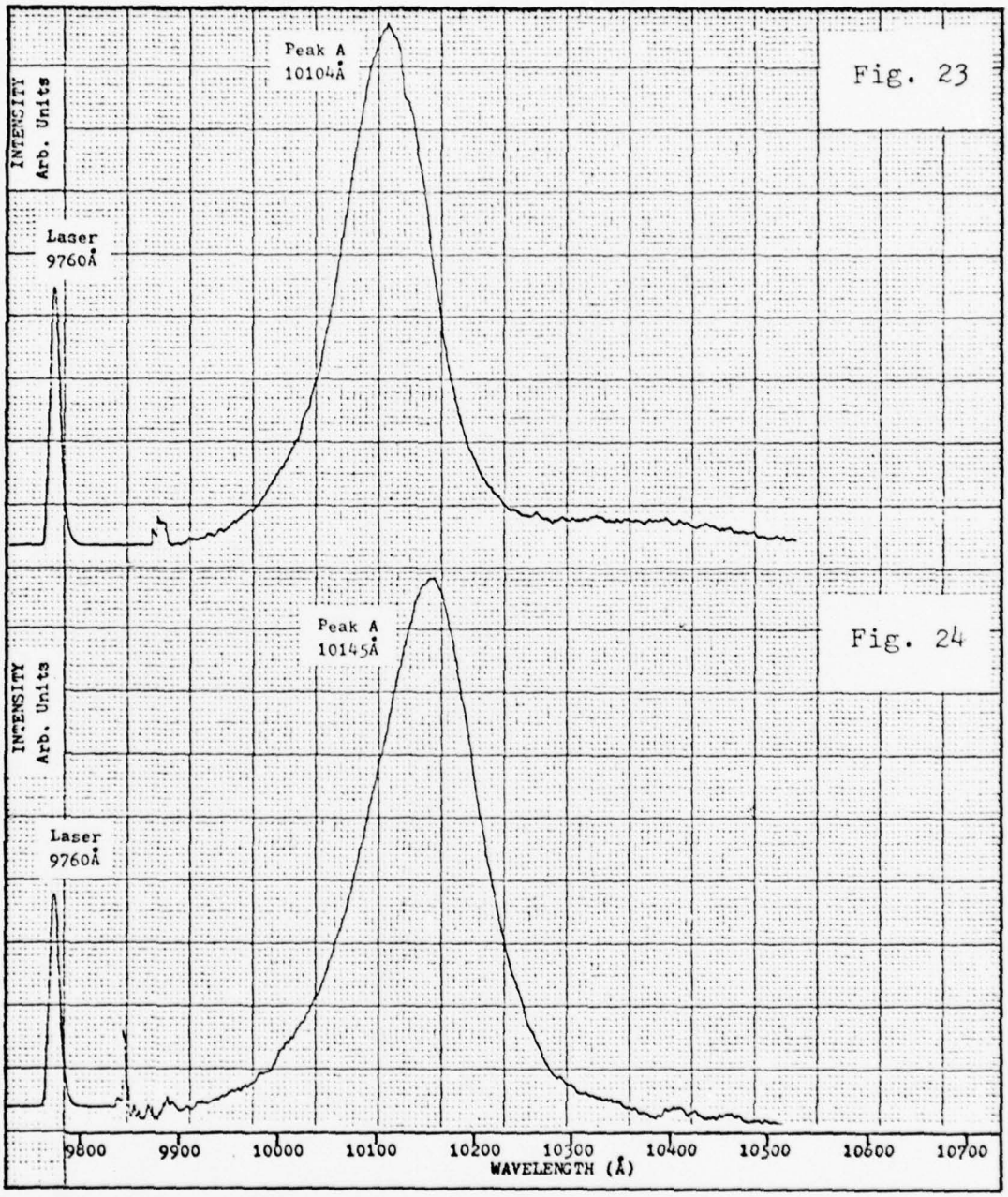

Fig. 23. QF 3003 at 60°K

Fig. 24. QF 3003 at 90°K

Sample QF 3003. The two emission peaks observed in this sample are illustrated in Fig. 19 for 4.2°K. Peak A is 9 meV wide and is situated at 1.230 eV. The smaller peak, peak B, is at 1.204 eV and is 22 meV wide.

By 10°K, peak A has greatly increased in size with respect to peak B (Fig. 20). Peak widths and positions are basically unchanged. Between 10°K and 30°K, peak A slowly widens but does not shift its position. Peak B, however, begins to shift toward longer wavelengths at about 20°K.

At a temperature of 28°K, peak B has shifted to 1.202 eV and widened to 23.5 meV (Fig. 21). Peak A, still the larger peak, has widened to 10 meV, but remains unchanged otherwise. By 45°K, peak A has started to shift toward longer wavelengths (Fig. 22). Peak B has reached 1.198 eV, where it remains as the temperature rises further. Peak B is barely visible as a low mound on the long wavelength side of peak A.

Between 45°K and 90°K, peak A continues to grow wider and to move toward longer wavelengths. Peak B vanishes at 60°K, leaving peak A as the only remaining feature of the emission spectrum (Fig. 23). When the temperature has reached 90°K, peak A has shifted to 1.222 eV and is 15.6 meV wide (Fig. 24). Peak A is only one-twentieth the size it was at 10°K.

The peak location, peak height, and half-width as functions of temperature are illustrated graphically in Figs. 25, 26, and 27 respectively.

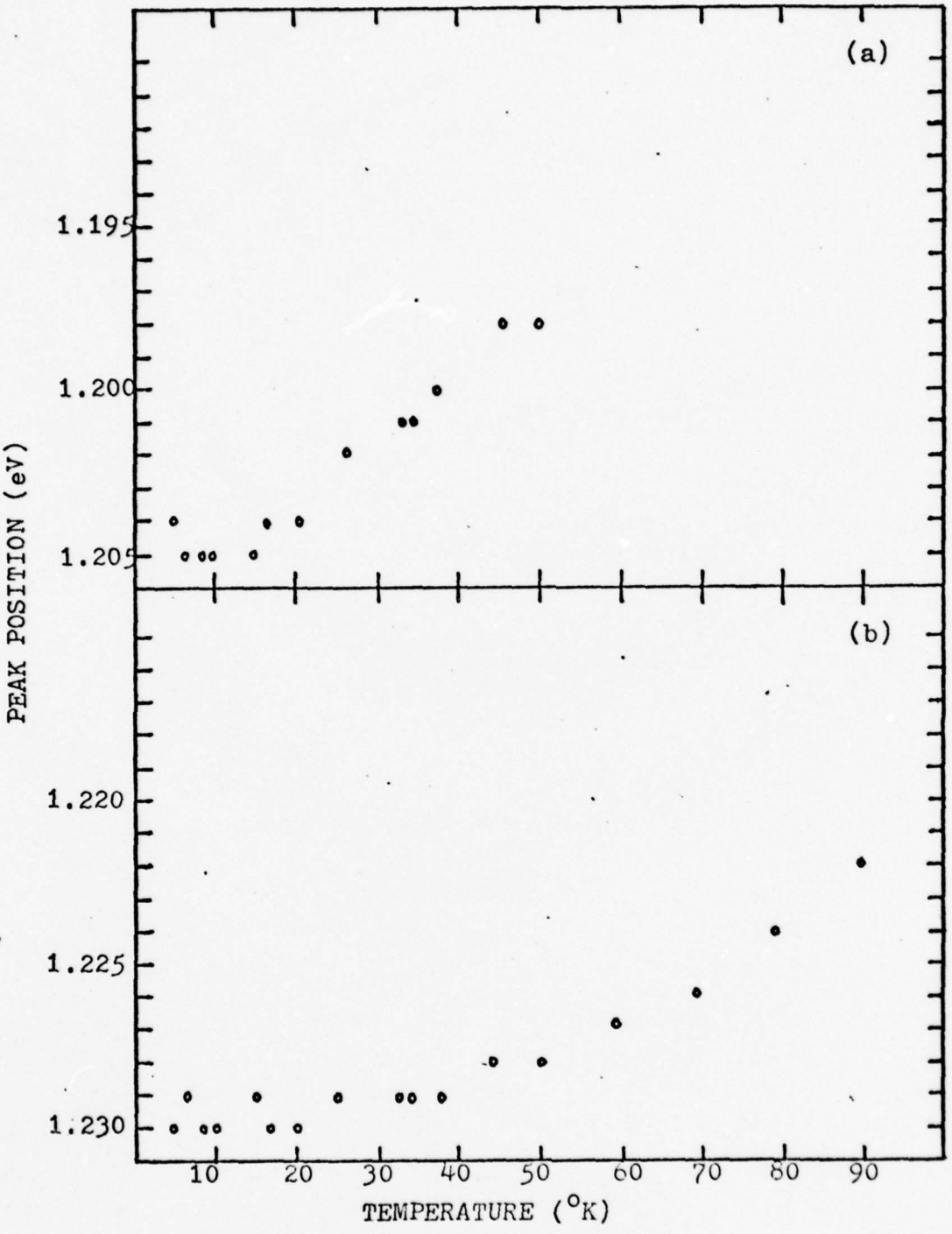

Fig. 25. QF 3003: Peak position as a function of temperature for peak B (a) and peak A (b)

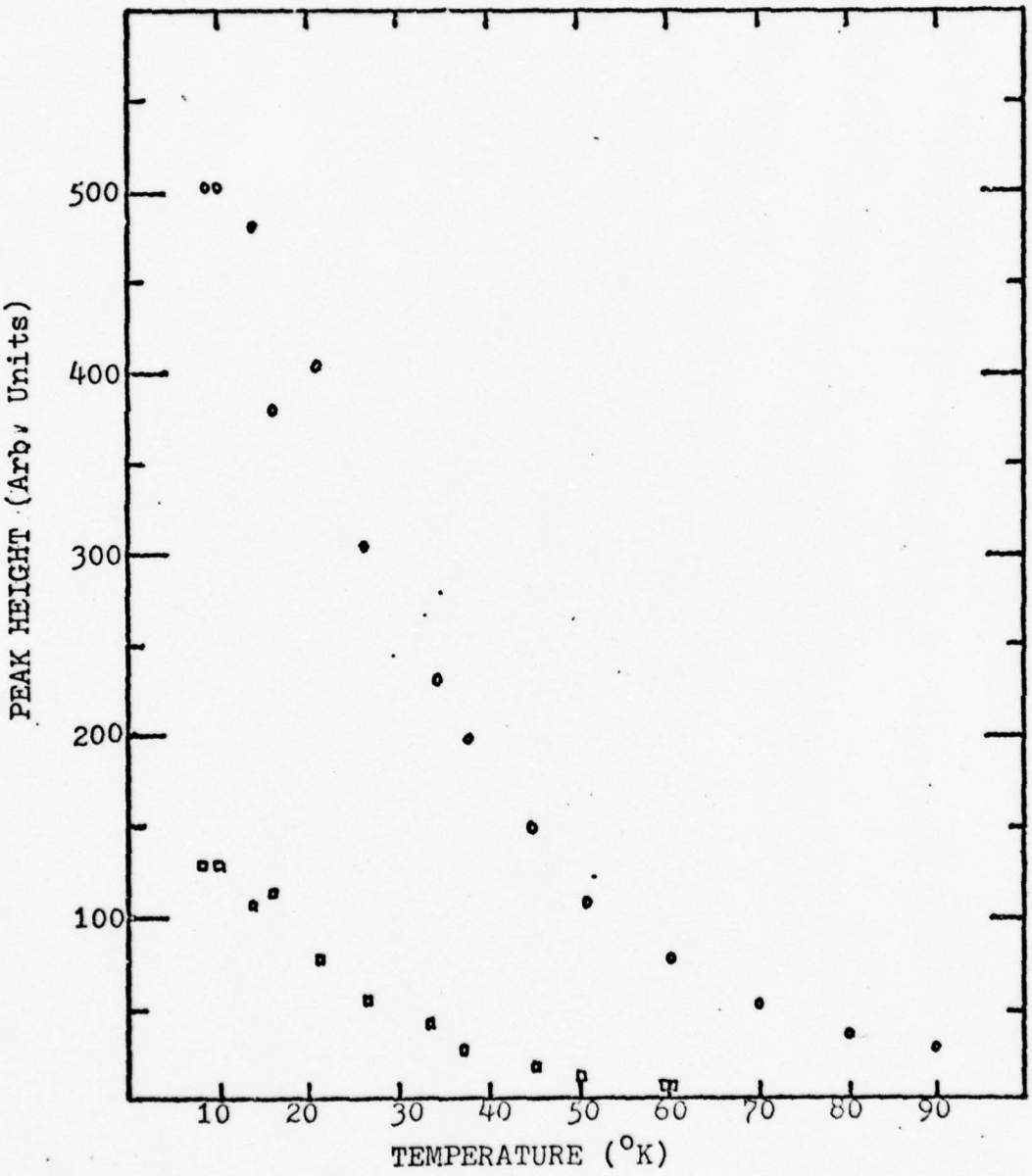

Fig. 26. QF 3003: Variation of peak height with temperature for peak A (•) and peak B (□)

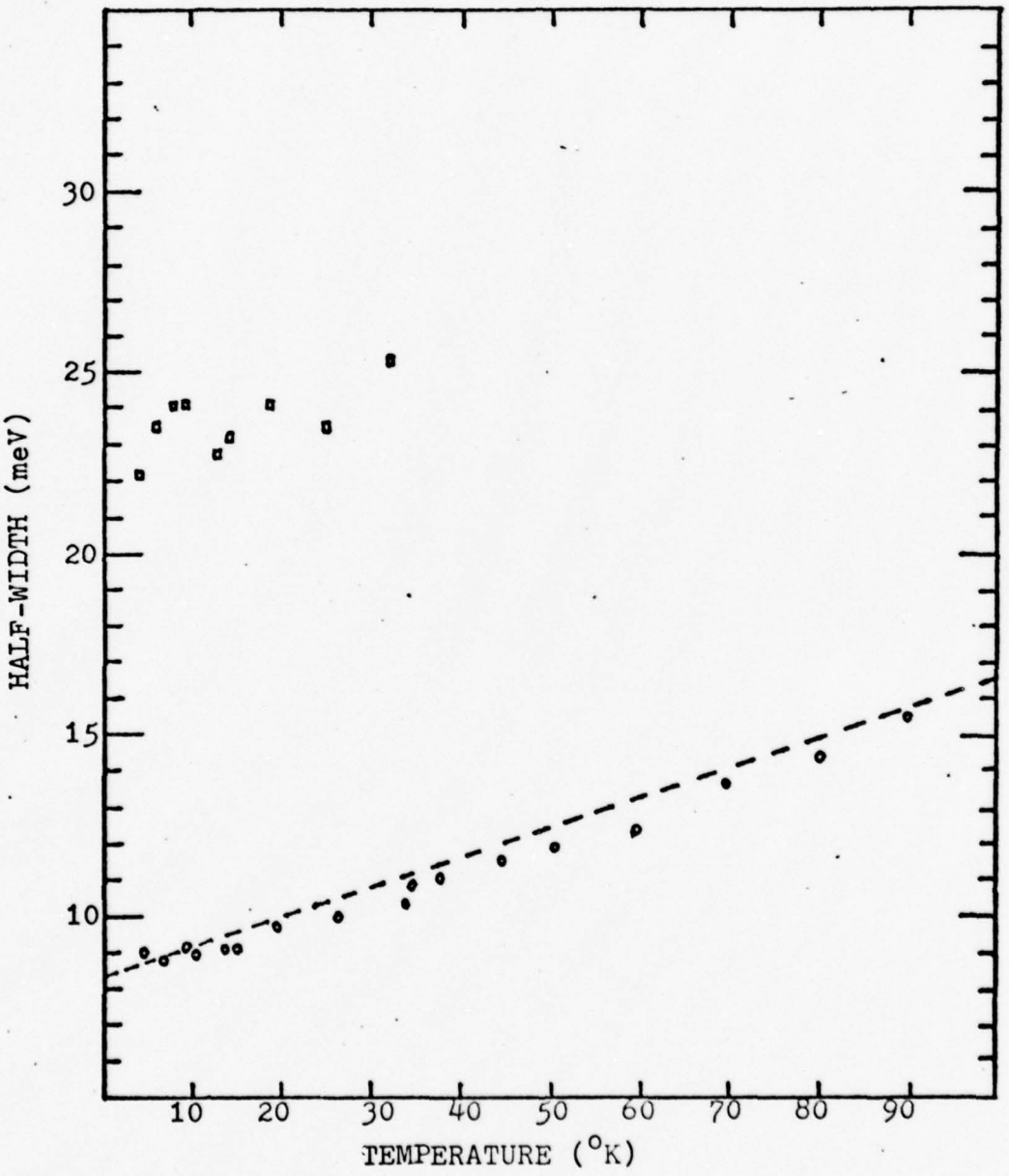

Fig. 27. QF 3003: Variation of half-width (full width at half maximum) with temperature for peak A (°) and peak B (□). The dotted line has a slope equal to "k", the Boltzmann constant

The carrier concentration in sample QF 3003 is only 10% of what it was in sample Q 2945/106. This change in carrier concentration is undoubtedly the reason for the sudden decrease of peak B with respect to peak A (Fig. 26). Fewer impurity atoms implies less donor-acceptor pair recombination. The half-width variation and temperature quenching (Figs. 26, 27) of peak B are consistent with donor-acceptor pair recombination. Peak B begins to shift toward longer wavelength at about 20°K, then slows its shift near 45°K (Fig. 25). This behavior is consistent with donor-acceptor pair recombination (Ref 41:281).

Peak A is the result of free-to-bound recombination. The peak widens as kT (Fig. 27) and shifts linearly toward higher energies with respect to $E_G(0)$ as the temperature rises. Peak A dominates the emission spectrum at high temperatures (77°K), as is expected in a free-to-bound peak.

Sample Q 2601-0. At 6.6°K, the emission spectrum consists of a tall, narrow peak (A) at 1.276 eV with a second peak (B) appearing as a low energy shoulder at 1.267 eV (Fig. 28). Peak A is 7.3 meV wide.

By 20°K, peak B has become nearly indistinguishable (Fig. 29). Peak A has widened to 8.4 meV, but is still located at 1.276 eV.

At 30°K, peak B no longer appears in the emission spectrum, but peak A has developed a low energy shoulder one meV below its summit (Fig. 30). The width of peak A is 9.2 meV.

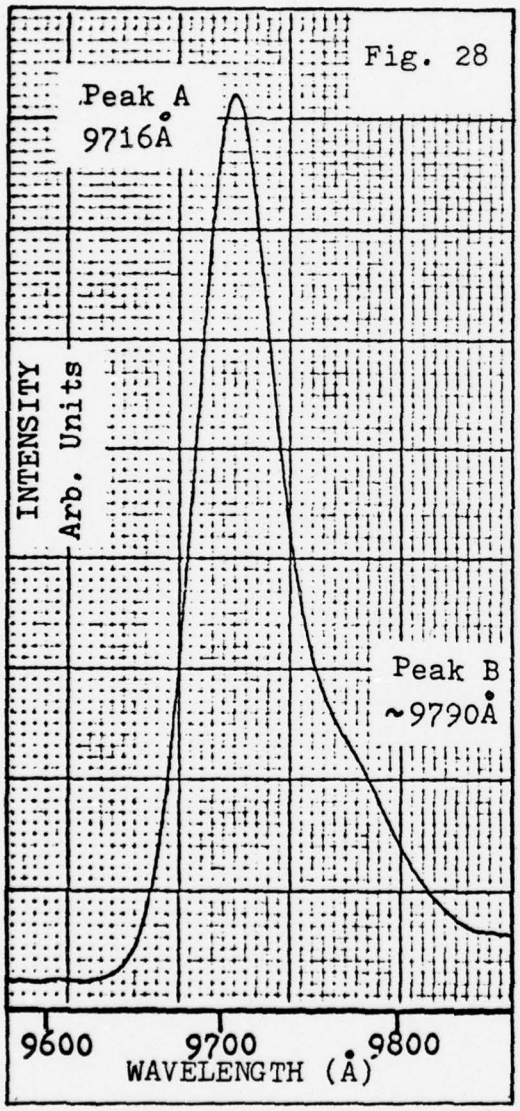

Fig. 28. Q 2601-0 at 6.6°K

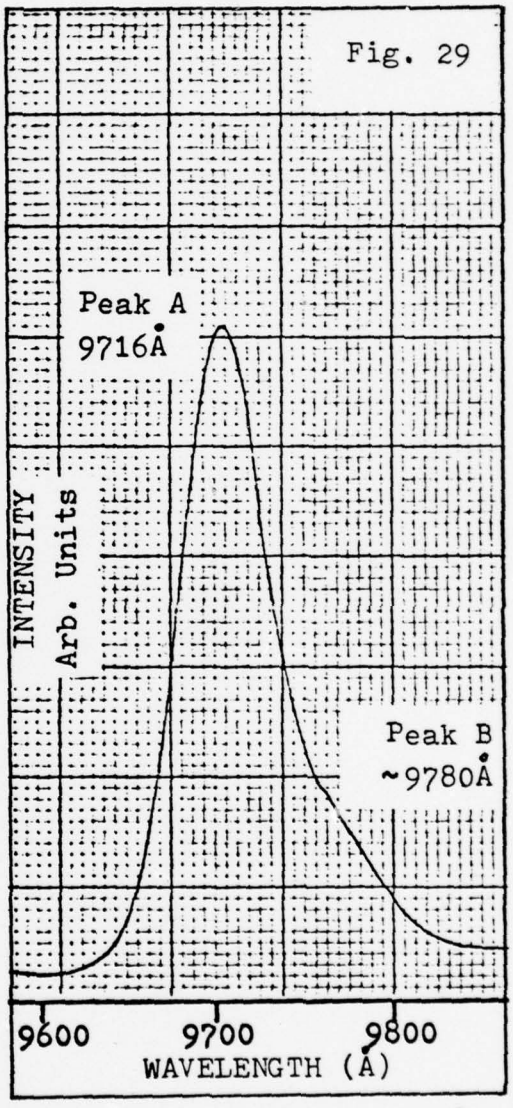

Fig. 29. Q 2601-0 at 20°K

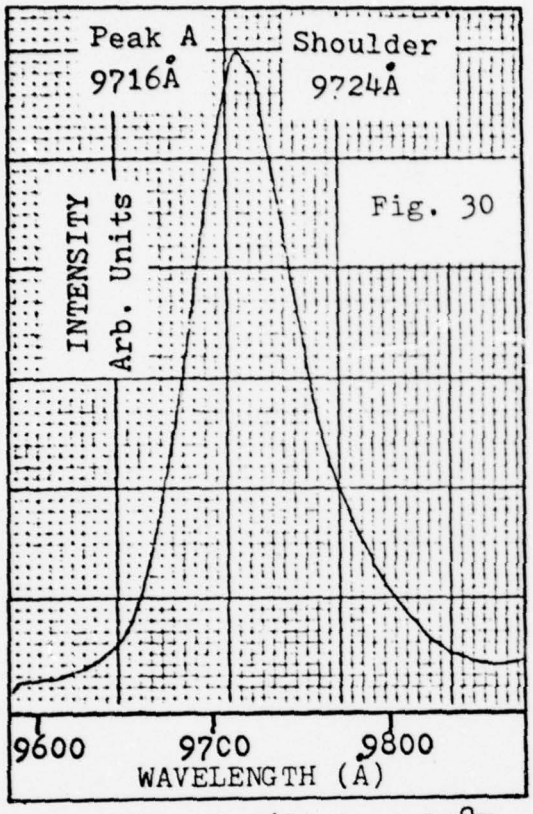

Fig. 30. Q 2601-0 at 30°K

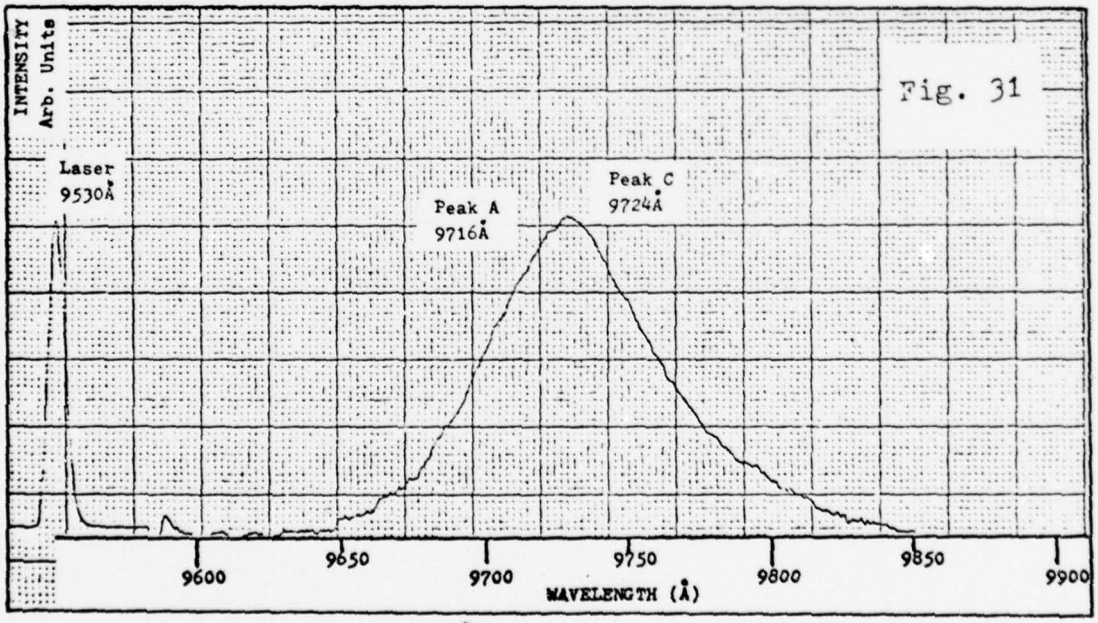

Fig. 31. Q 2601-0 at 40°K

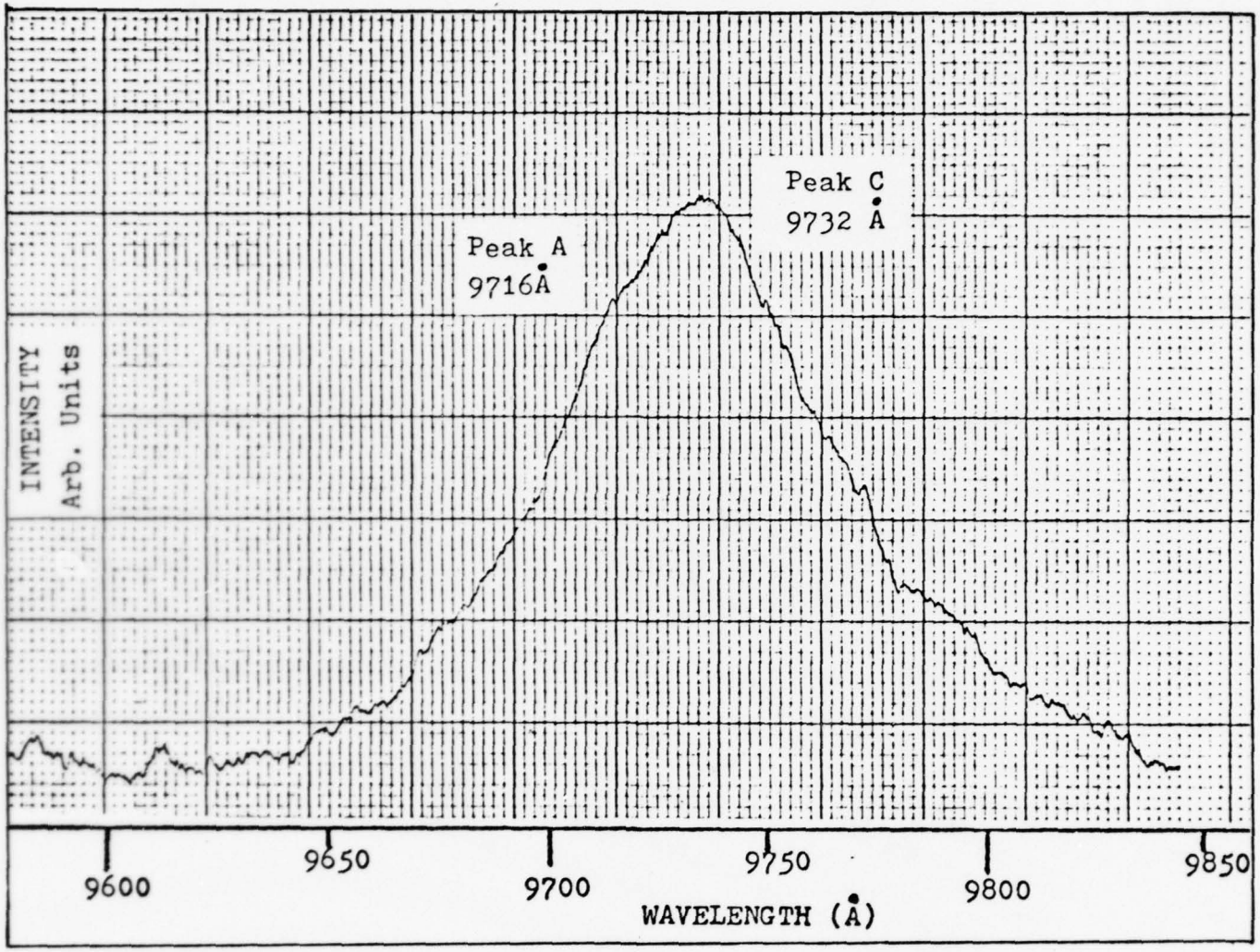

Fig. 32. Q 2601-0: An expanded view of peak A at 50°K

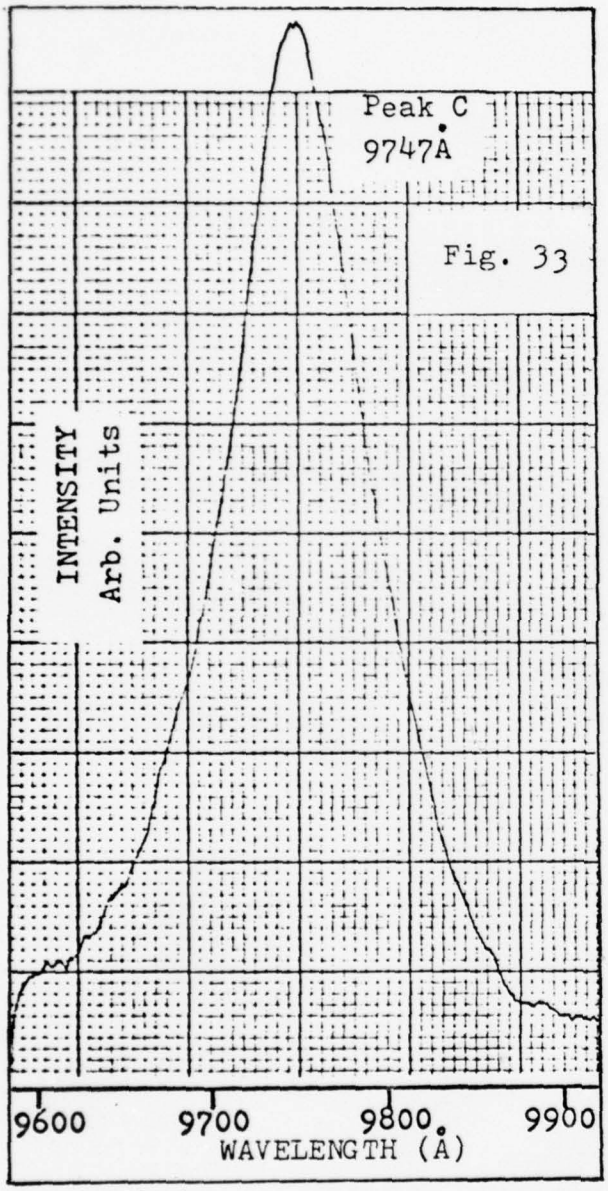

Fig. 33. Q 2601-0 at 70°K

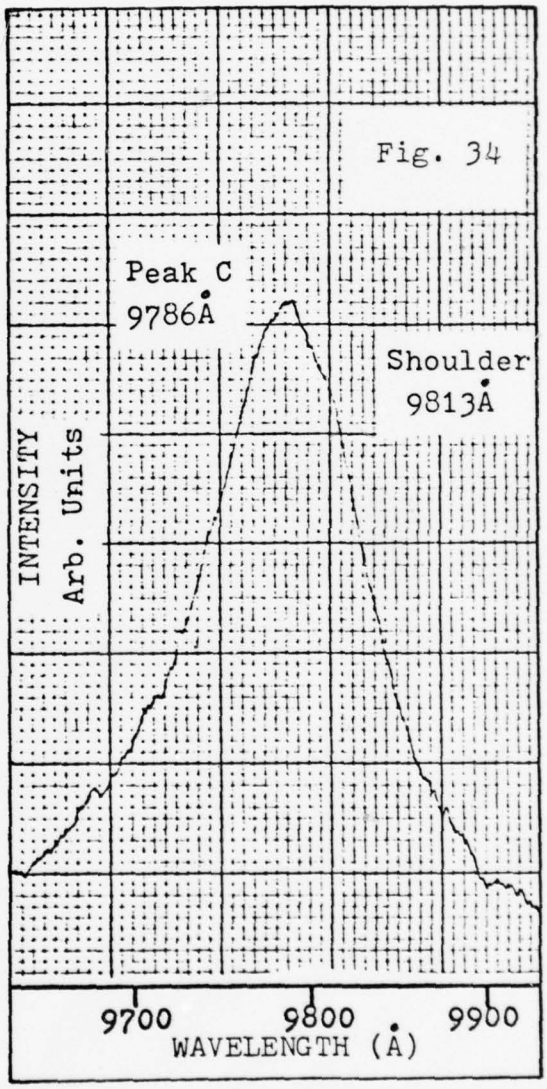

Fig. 34. Q 2601-0 at 100°K

Fig. 31 is an expanded view of peak A at 40°K. Peak A now appears to have a high energy shoulder one meV above the summit. A close examination of the position of this shoulder reveals that it is probably the former summit of peak A which has diminished with respect to the low energy shoulder that existed at 30°K. Henceforth, the high energy shoulder shall be called "peak A" and the former low energy shoulder (now the summit) shall be called "peak C."

At 50°K, the high energy shoulder (peak A) is located at 1.277 eV, one meV below its location at 20°K (Fig. 32). Peak C has moved toward longer wavelength, and is now at 1.274 eV. The width of the combination peak (A + C) is 10.3 meV.

By 70°K, peak A is only visible as a slight change in slope on the high energy side of peak C (Fig. 33). Peak C is 12.6 meV wide and has moved to 1.272 eV.

At 100°K, peak C has widened to 14.5 meV. It has shifted to 1.266 eV and gained a low energy shoulder of unknown origin at 1.263 eV (Fig. 34).

The temperature dependence of peak shift for peaks A and C is illustrated in Fig. 35. Fig. 36 illustrates the quenching of peaks A, B, and C, and Fig. 37 depicts the half-width variation of peaks A and C as a single unit.

Peak B is probably due to donor-acceptor pair recombination. The small size of peak B in this sample is the result of the purity of sample Q 2601-0. Since peak B quenches very rapidly and soon vanishes from the emission spectrum, there is scant evidence to support this hypothesis.

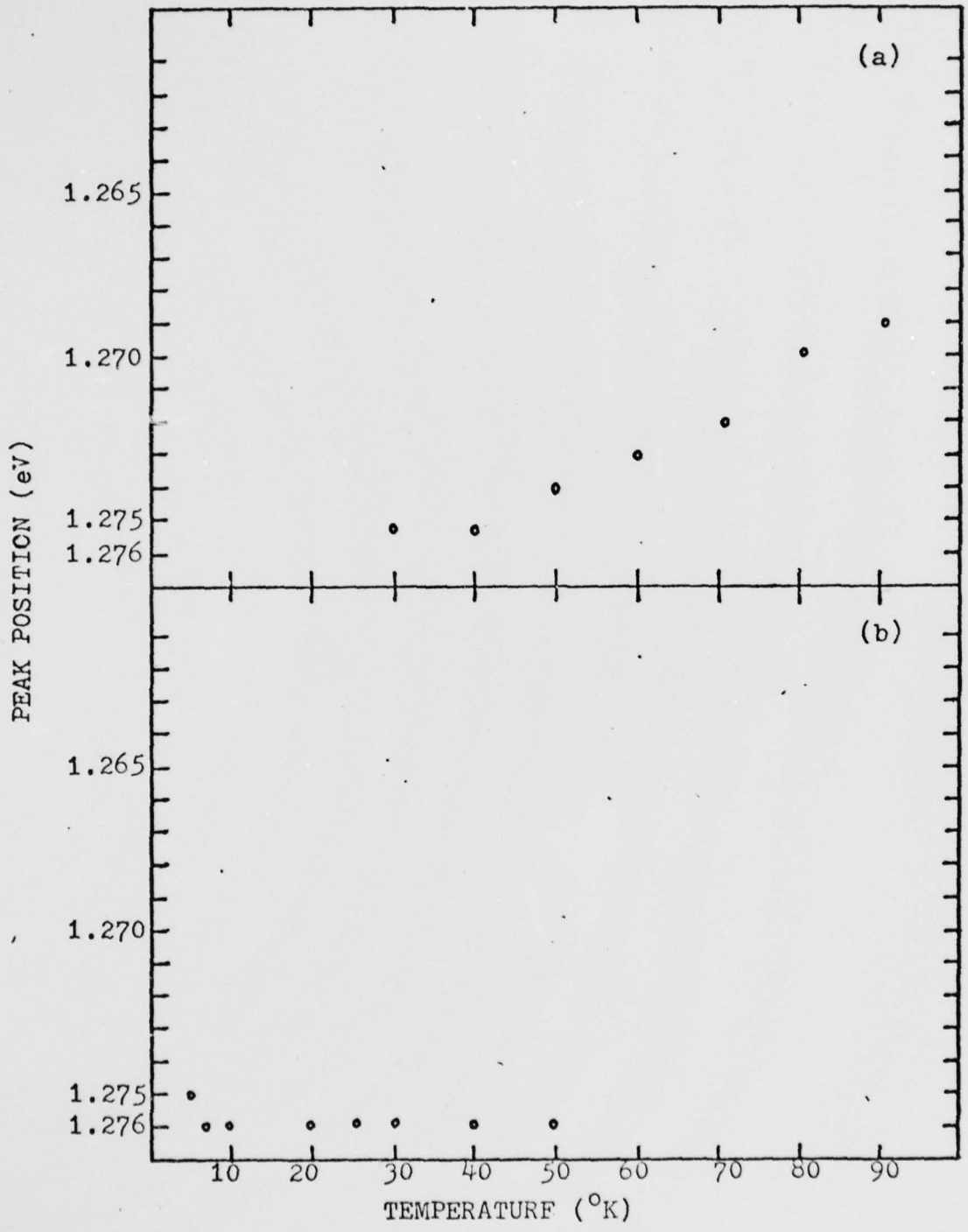

Fig. 35. Q 2601-0: Peak position as a function of temperature for peak C (a) and peak A (b)

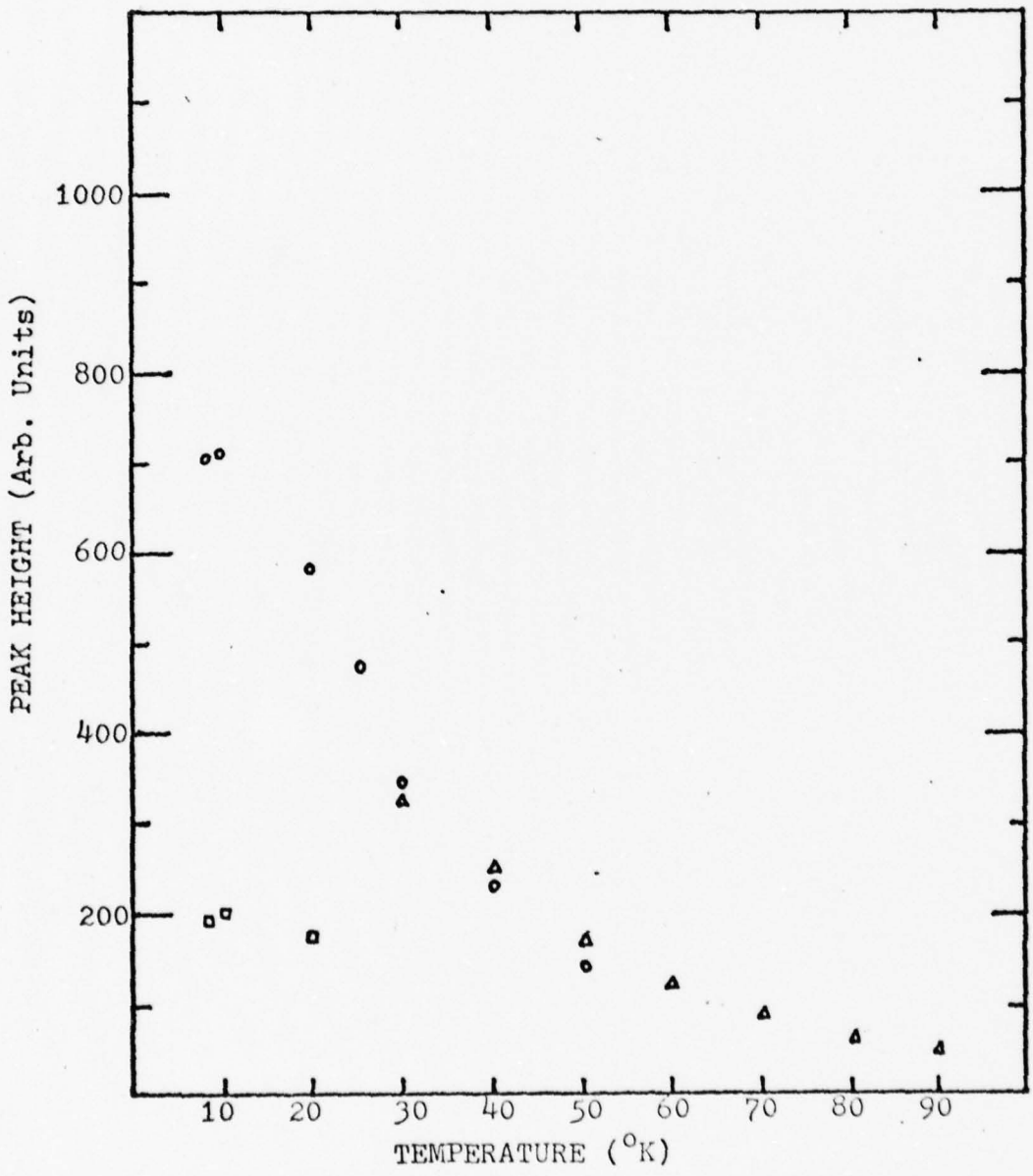

Fig. 36. Q 2601-0: Variation of peak height with temperature for peak A (o), peak B (□), and peak C (Δ)

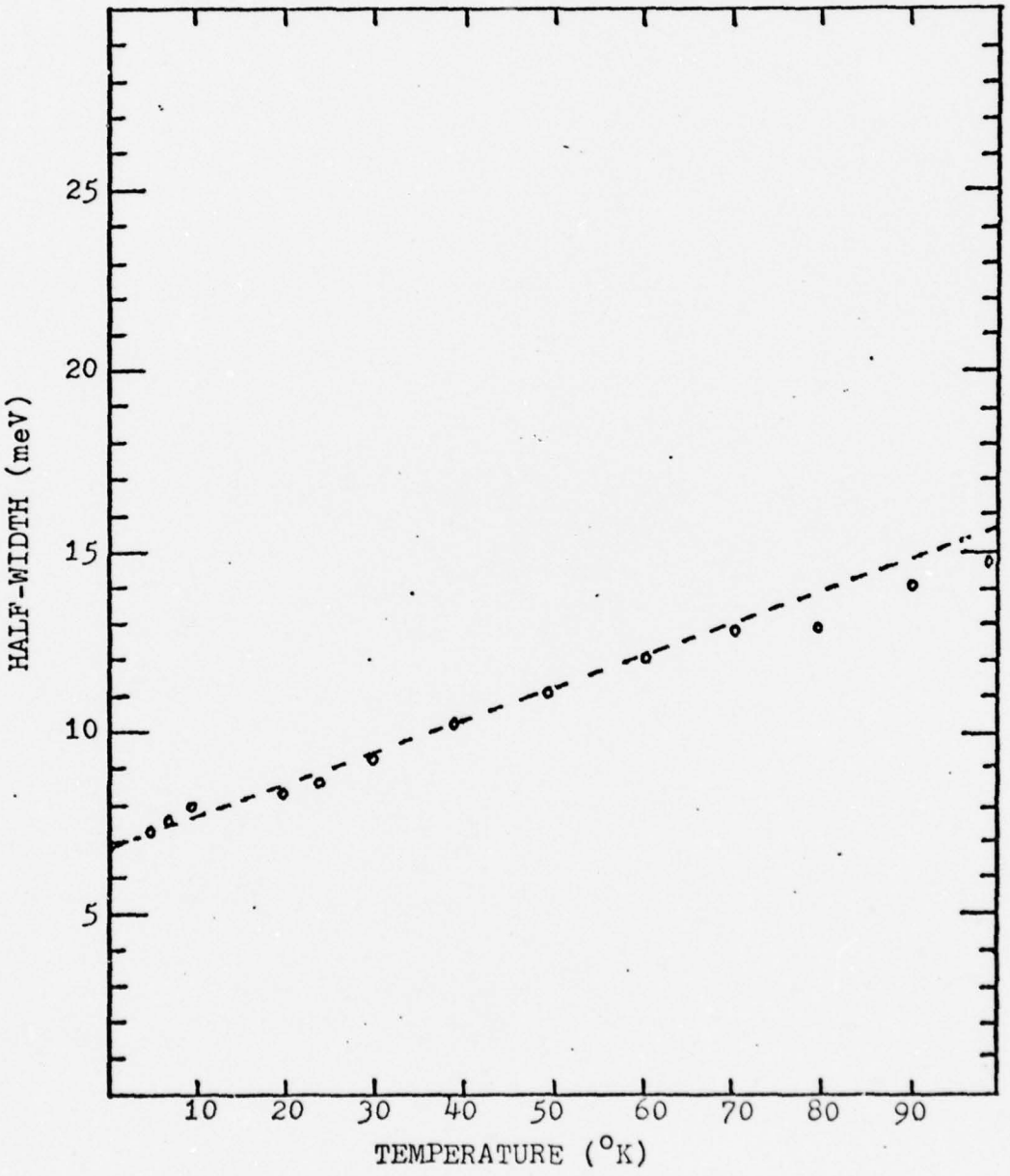

Fig. 37. Q 2601-0: Variation of half-width (full width at half maximum) with temperature for peak A and peak C as a unit. The dotted line has a slope equal to "k", the Boltzmann constant

Both peak A and peak C would seem to be due to free-to-bound recombination. The two peaks widen as kT (Fig. 37), and peak C is the dominant spectral feature at high temperatures. Both peaks shift linearly toward higher energies with respect to $E_G(0)$ as the temperature rises. Evidently somewhere in the vicinity of $40^{\circ}K$, the electrons of the crystal are funneled out of the impurity level associated with peak A to a nearby impurity level associated with peak C. These two impurity levels are so close together that as the temperature rises still further, peak A vanishes into the high energy side of peak C. The low energy shoulder that appears on peak C above $90^{\circ}K$ appears in only one plot of the emission spectrum and cannot be explained due to a lack of data.

Sample 6-1A. Sample 6-1A is LPE InP grown on an InP substrate. The bandgap at absolute zero is 1.423 eV (Ref 25). The room temperature carrier concentration is about 5×10^{15} cm^{-3}.

At $4.2^{\circ}K$, the emission spectrum consists of a narrow (6.3 meV) peak at 1.417 eV with a low energy shoulder at 1.415 eV; a broader peak (8.5 meV) at 1.380 eV; and a small peak at about 1.337 eV (Fig. 38).

By $20^{\circ}K$, the low energy shoulder has vanished from the narrow peak (D). The broader peak (E) and the small peak (F) are unchanged (Fig. 39).

Five degrees later, at $25^{\circ}K$, peak E has suddenly increased in size with respect to peak D (Fig. 40). None

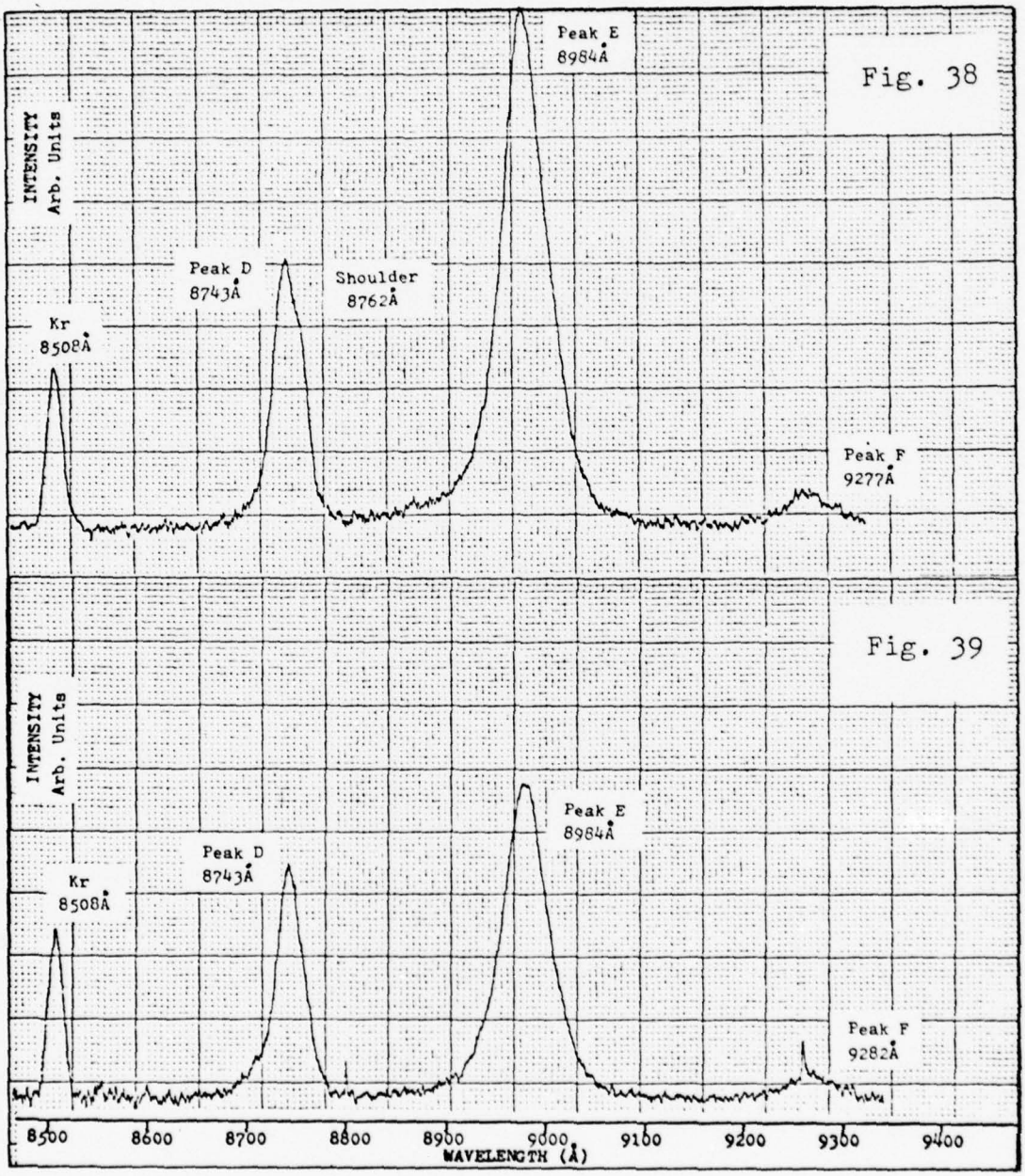

Fig. 38. 6-1A at 4.2°K

Fig. 39. 6-1A at 20°K

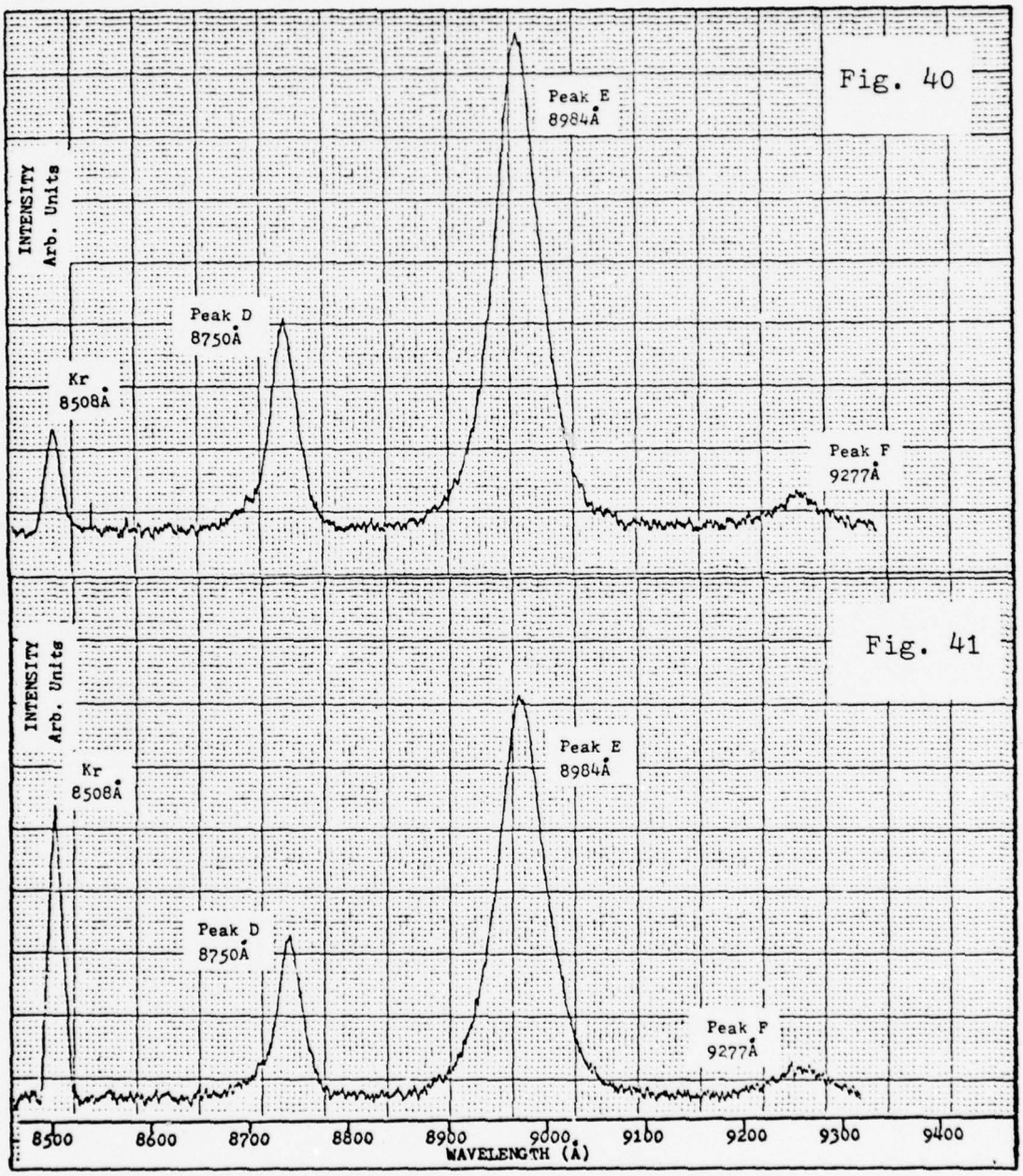

Fig. 40. 6-1A at 25°K

Fig. 41. 6-1A at 30°K

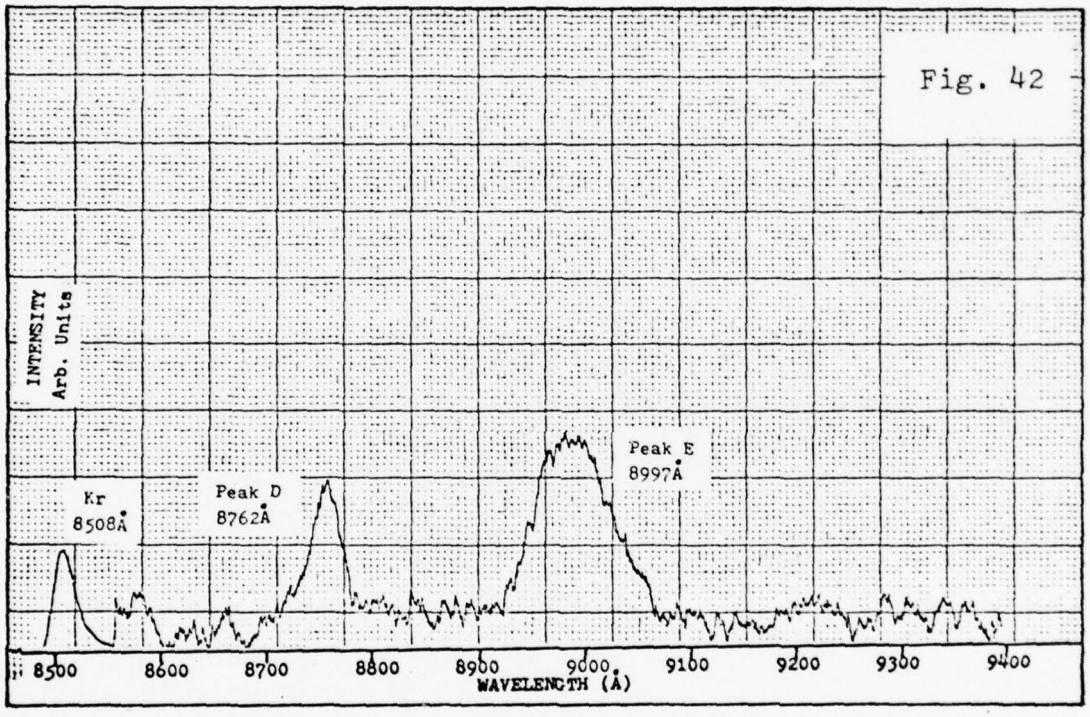

Fig. 42. 6-1A at 50°K

of the peaks have shifted location or widened.

At 30°K, peak E has begun to decrease in size again (Fig. 41). Otherwise, the emission spectrum remains unchanged. At about 40°K, all of the peaks start to shift very slowly toward longer wavelength, with peak F staying 43 meV below peak E.

At 50°K, peak F is gone. Peaks D and E are of equal height, and have both shifted about 2 meV toward longer wavelength (Fig. 42).

Peak location, height, and half-width as they vary with temperature are plotted for peaks D and E in Figs. 43, 44, and 45 respectively. The behavior of peak F is the same as that of peak E.

Peak F is a phonon replica of peak E. The energy separation between peaks E and F is always equal to the longitudinal optical phonon energy of 43 meV (Ref 28:157).

Peak E quenches rapidly with temperature (Fig. 43) and otherwise acts like a donor-acceptor pair band. Even the peak shift with respect to temperature is consistent with this hypothesis, which is supported by Heim (Ref 18: 542). Recent work by E. W. Williams suggests that peak E is somehow associated with zinc acceptors (Ref 48:1742).

The structure in peak D is difficult to resolve even at low temperatures. The resolution of this tightly bound area is the real test of the experimental apparatus. The summit called "peak D" acts like an exciton-caused peak, and has been so identified by Heim (Ref 18:543). Of the remaining structure seen by Heim in the same wavelength

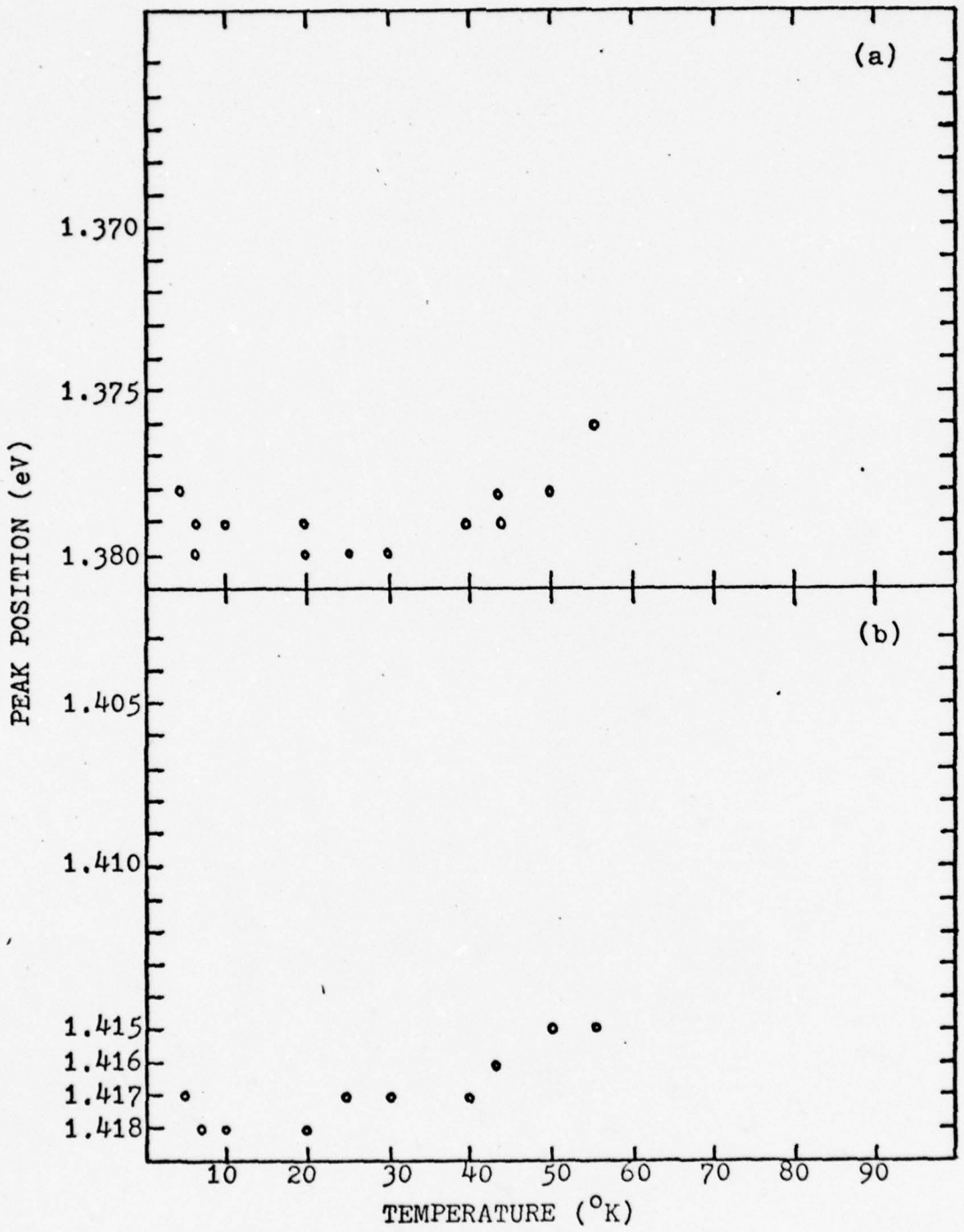

Fig. 43. 6-1A: Peak position as a function of temperature for peak E (a) and peak D (b)

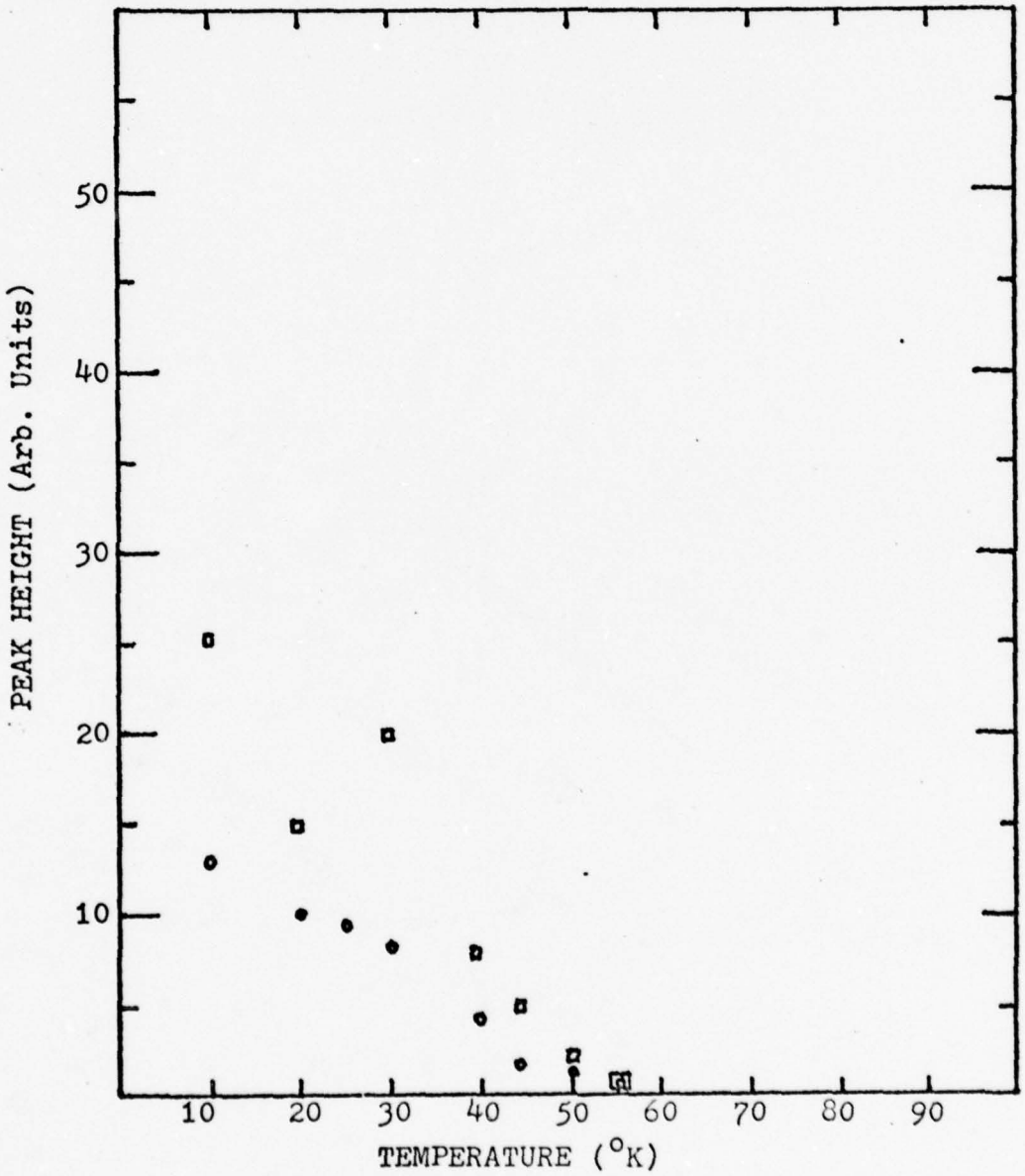

Fig. 44. 6-1A: Variation of peak height with temperature for peak D (◦) and peak E (□)

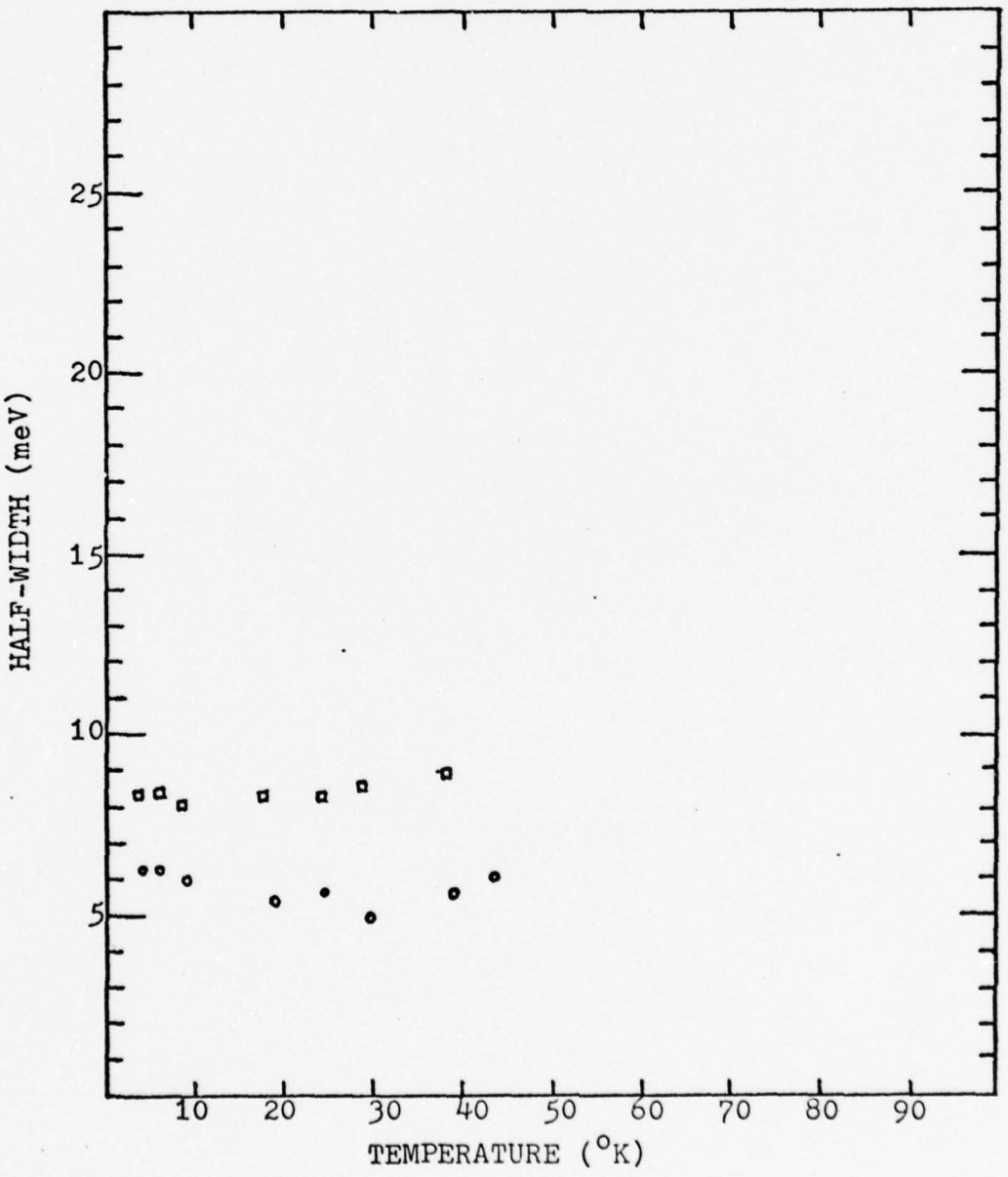

Fig. 45. 6-1A: Variation of half-width (full width at half maximum) with temperature for peak D (o) and peak E (□)

region as peak D, only a shoulder at 1.415 eV is visible. This shoulder is probably Heim's 1.414 eV bound-exciton peak, but it vanishes so swiftly with increasing temperature that it is not possible to prove this. Neither Heim's high energy shoulder at 1.418 eV nor his peak at 1.4123 eV are seen. This leads to the conclusion that the resolution of the experimental apparatus used in this study (one meV) is insufficient for the examination of fine structure.

Summary

The half-width and energy of the peaks in each of the GaInAsP samples are listed in Table II at 6.6°K and 90°K. Also included in Table II are the half-width and energy of the peaks of the InP sample at 4.2°K and 50°K. These numbers are intended as representative values only. Exact information may be obtained from the graphs appearing earlier in this thesis.

Table II. Features of the GaInAsP and InP Spectra					
Sample Number	Peak	(meV) Half-Width (6.6°K)	(meV) Half-Width (90°K)	(eV) Peak Energy (6.6°K)	(eV) Peak Energy (90°K)
Q 2945/106	A	17.7	26.0	1.072	1.069
	B	32.0	-	1.057	-
QF 3003	A	8.6	15.6	1.230	1.222
	B	23.4	-	1.205	-
Q 2601-0	A	7.6	-	1.276	-
	B	?	-	1.267	-
	C	-	13.7	-	1.269
		(4.2°K)	(50°K)	(4.2°K)	(50°K)
6-1A	D	6.3	6.3	1.417	1.415
	Shoulder	?	-	1.415	-
	E	8.5	12.0	1.377	1.376
	F	*7.0	-	*1.336	-

"-" indicates that no value exists at this point
"?" indicates an unmeasureable quantity

*(this value taken at 6.6°K)

V. Conclusions and Recommendations

The emission spectrum of these LPE GaInAsP wafers grown on InP substrates has been found to consist of a narrow, near-band edge peak that behaves like a free-to-bound recombination peak and a broad, donor-acceptor pair band. The donor-acceptor pair band is especially useful as an indicator of the carrier concentration of a sample, since this peak noticeably reduces in size with respect to the near-band edge peak as the carrier concentration decreases.

Earlier photoluminescent studies associated an emission peak in the region of 0.68 eV-0.78 eV and a broad band stretching from 0.925 eV-1.17 eV with the presence of deep defects in the epilayer (Ref 17:20). That these peaks were not found is a clear indication of the crystalline perfection of the wafers studied. However, the peak widths of the emission spectrum of the pure InP sample (6-1A) were significantly narrower than those in the emission spectra of the GaInAsP samples. It is impossible to tell how deep within the GaInAsP epilayers electron-hole pairs are being created, since the absorption length of argon laser light in GaInAsP is not known. We cannot even know whether radiation is reaching the observer from the substrate-epilayer interface. The widening of the GaInAsP emission peaks could be the result of lattice mismatch at that interface, or it could be due to compositional variation within the GaInAsP epilayers, or to sublattice disorder. Whichever reason is the right one, the GaInAsP epilayers are not

as perfect as the InP epilayer.

Recommendations

This investigation was severely handicapped because the bandgap variation with temperature was not known. Photoluminescence is sensitive to impurities which yield transition energies below the bandgap, while absorption or reflectance measurements yield information about the extent of the bandgap itself. Once the variation of the bandgap with temperature is known, it will be much easier to determine the activation energies of the impurities present in GaInAsP samples.

Several methods could be used to verify that peak B is indeed the result of donor-acceptor pair recombination. Time resolved spectroscopy has often been used to identify the cause of emission peaks (Ref 39). A change in excitation intensity produces unique changes in the position of donor-acceptor pair bands.

To further investigate the nature of peak A, an external magnetic field could be applied to a GaInAsP sample. The nature of the resulting line splitting would help determine whether or not peak A is a free-to-bound peak.

The sample with the broadest emission peaks, and therefore with the poorest crystalline properties, was sample Q 2945/106. Was this the result of unintentional doping, or was it because this particular sample was grown on a [11] B crystalline face of InP? Further studies of GaInAsP might look into this.

The sample with the lowest carrier concentration (Q 2601-0) exhibited poorly resolved fine structure in the near-band edge peak. It is possible that such fine structure exists in the other emission spectra as well. It would be worthwhile to examine samples of epitaxial GaInAsP with an experimental system capable of greater resolution that the system employed in this investigation.

Bibliography

1. Antypas, G. A., et al. "III-V Quaternary Alloys," In 1972 Symposium on GaAs. 48-54.

2. Antypas, G. A. and R. L. Moon. "Growth and Characterization of InP-InGaAsP Lattice-Matched Heterojunctions," Electrochemical Society Journal, 120: 1574-1577 (November 1973).

3. Antypas, G. A. and L. Y. L. Shen. "Orientation Dependence of the Incorporation of Ga, As, and Zn during LPE Growth of InGaAsP Alloys," In 1977 Symposium on GaAs. 96-104.

4. Bell, R. L. "Varian Proposal 2278-Advanced III-V Compound Microwave Device Investigation." Response to Air Force Solicitation #F33615-77-R-1037. Palo Alto, California: Varian Associates, December 1976.

5. Bogardus, E. H. and H. B. Bebb. "Bound-Exciton, Free-to-Bound, Band-Acceptor, Donor-Acceptor, and Auger Recombination in GaAs," Physical Review, 176: 993-1002 (15 December 1968).

6. Colbow, K. "Free-to-Bound and Bound-to-Bound Transitions in CdS," Physical Review, 141: 742-749 (January 1966).

7. Dexter, D. L. and R. S. Knox. Excitons. New York: John Wiley and Sons, Inc., 1965.

8. Dingle, R. "Radiative Lifetime of Donor-Acceptor Pairs in p-type Gallium Arsenide," Physical Review, 184: 788-796 (15 August 1969).

9. Dolginov, L. M., et al. "High-Efficiency Electroluminescence of $Ga_xIn_{1-x}As_{1-y}P_y$," Soviet Physics Semiconductors, 9: 871-873 (July 1975).

10. Dolginov, L. M., et al. "Energy Band Diagram of InP-$Ga_xIn_{1-x}As_{1-y}P_y$ Heterojunctions," Soviet Physics Semiconductors, 10: 729 (June 1976).

11. Dolginov, L. M., et al. "Spontaneous and Stimulated Emission from $Ga_xIn_{1-x}As_{1-y}P_y$, $Ga_xIn_{1-x}As$, and $GaAs_xSb_{1-x}$ Solid Solutions," Soviet Journal of Quantum Electronics, 6: 1367-1369 (November 1976).

12. Escher, J. S., et al. "High-Quantum-Efficiency Photoemission from an InGaAsP Photocathode," Applied Physics Letters, 29: 153-154 (1 August 1976).

13. Hagston, W. E. "A Unified Treatment of the Theory of Donor-Acceptor Pair Recombination Emission," Journal of Luminescence, 5: 285-296 (1972).

14. Halperin, A. and E. Zacks. "Temperature Dependence of the 2.2-eV Pair-Recombination Band in GaP(S,C) Crystals," Physical Review B, 11: 2237-2242 (12 March 1975).

15. Harrison, J. W. and J. R. Hauser. "Alloy Scattering in Ternary III-V Compounds," Physical Review B, 13: 5347-5350 (15 June 1976).

16. Harrison, J. W., et al. "Advanced III-V Compound Materials Study." Final Report on Contract #F33615-76-C-1265. Research Triangle Park, North Carolina: Research Triangle Institute, 1977.

17. Harrison, J. W., et al. "Quaternary Alloy Microwave MESFET." Annual Technical Report on AFOSR Contract #F49620-77-C-0062. Research Triangle Park, North Carolina: Research Triangle Institute, February 1978.

18. Heim, V., et al. "Photoluminescence of InP," Journal of Luminescence, 1 & 2: 542-552 (1970).

19. Hitchens, W. R., et al. "Low Threshold LPE in $In_{1-x}Ga_xP_{1-z}As_z/In_{1-x}Ga_xP_{1-z}As_z/In_{1-x}Ga_xP_{1-z}As_z$ Yellow Double-Heterojunction Laser Diodes," Applied Physics Letters, 27: 245-247 (15 August 1975).

20. Hsieh, J. J. "Room-Temperature Operation of GaInAsP/InP Double-Heterojunction Diode Lasers Emitting at 1.1 μm," Applied Physics Letters, 28: 283-285 (1 March 1976).

21. Hsieh, J. J., et al. "Room-Temperature CW Operation of GaInAsP/InP Double-Heterojunction Diode Lasers Emitting at 1.1 μm," Applied Physics Letters, 28: 709-711 (15 June 1976).

22. Hsieh, J. J., et al. "Conditions for Lattice-Matching in the LPE Growth of GaInAsP Layers on InP Substrates," Institute of Physics Conference, Serial No. 33b: 37-43 (1977).

23. James, L. W., et al. "Photoemission from Cesium-Oxide-Activated InGaAsP," Applied Physics Letters, 22: 270-271 (15 March 1973).

24. Kennedy, J., et al. "InP-An Assessment of U.S. Activities," Unpublished. Written for NATO Symposium on Microwave Components for the Region Above 6 Ghz. January 1978.

25. Kittel, C. Introduction to Solid State Physics. New York: John Wiley and Sons, Inc., 1976.

26. Ku, San-mei and J. F. Black. "Injection Electroluminescence in GaAs-GaP Diodes," Solid State Electronics, 6: 505-509 (July/August 1963).

27. Leite, R. C. and A. E. DiGiovanni. "Frequency Shift with Temperature as Evidence for Donor-Acceptor Pair Recombination in Relatively Pure n-type GaAs," Physical Review, 153: 841-843

28. Leite, R. C. "Radiative Recombination in n-type InP," Physical Review, 157: 672-676 (15 May 1967).

29. Littlejohn, M. A., et al. "Velocity-field Characteristics of $Ga_{1-x}In_xP_{1-y}As_y$ Quaternary Alloys," Applied Physics Letters, 30: 242-244 (1 March 1977).

30. Madelung, Ottfried. Physics of III-V Compounds. New York: John Wiley and Sons, Inc., 1964.

31. Matthews, J. W. Epitaxial Growth, Pt. A. New York: Academic Press, 1975.

32. Moon, R. L., et al. "Bandgap and Lattice Constant of GaInAsP as a Function of Alloy Composition," Journal of Electronic Materials, 3: 635-644 (1974).

33. Morkoc, H., et al. "Advanced III-V Compound Microwave Device Investigation." Interim Technical Report on Contract #F33615-77-C-1037. Palo Alto, California: Varian Associates, May 1978.

34. Morkoc, H. Personal Communication, 22 September, 1978.

35. Muller, E. K. and John L. Richards. "Miscibility of III-V Semiconductors Studied by Flash Evaporation," Journal of Applied Physics, 35: 1233-1240 (April 1964).

36. Oirschot, T. G. J., et al. "Lattice Matching and Crystal Perfection in $Ga_yIn_{1-y}As_xP_{1-x}$ Heterojunctions," Institute of Physics Conference Series, No. 33b: 105-109 (1977).

37. Pankove, Jacques I. Optical Processes in Semiconductors. New York: Dover Publications, Inc., 1975.

38. Pearsall, T. P., et al. "Effective Lattice Matched Double-Heterojunction LEDs at 1.1 μm from $Ga_xIn_{1-x}As_yP_{1-y}$," Applied Physics Letters, 28: 499-500 (1 May 1976).

39. Pierce, Bruce. "Time Resolved Spectroscopy of ZnSe," Unpublished Thesis. Wright-Patterson AFB, Ohio: Air Force Institute of Technology, June 1969.

40. Pritchard, Harley H. "Photoluminescence of GaP," Unpublished Thesis. Wright-Patterson AFB, Ohio: Air Force Institute of Technology, April 1976.

41. Quiesser, H. J. "Advances in the Optical Analysis of Semiconductor Materials," Applied Physics, 10: 275-288 (August 1976).

42. Sankaran, G., et al. "Growth and Characterization of InGaAsP/InP Lattice Matched Heterojunctions," Journal of Vacuum Science Technology, 13: 932-937 (July/August 1976).

43. Thomas, D. G., et al. "Pair Spectra and 'Edge' Emission in GaP," Physical Review, 133: A269-A279 (6 January 1964).

44. Thomas, D. G., et al. "Light from Distant Pairs," In Radiative Recombination in Semiconductors, Paris 1964. New York: Academic Press, 1964.

45. Thomas, D. G. "An Account of Bound Excitons in Semiconductors," In Localized Excitations in Solids, edited by R. F. Wallis. New York: Plenum Press, 1968.

46. Willardson, R. K. and Albert C. Beer. Semiconductors and Semimetals, Vol. 2--Physics of III-V Compounds. New York: Academic Press, 1966.

47. Willardson, R. K. and Albert C. Beer. Semiconductors and Semimetals, Vol. 4--Physics of III-V Compounds. New York: Academic Press, 1968.

48. Williams, E. W., et al. "InP-1. A Photoluminescent Materials Study," Electrochemical Society Journal, 120: 1741-1749 (December 1973).

49. Williams, J. O. and P. J. Wright. "Growth and Characterization of Epitaxial $Ga_xIn_{1-x}As_yP_{1-y}$," Materials Research Bulletin, 12: 1227-1232 (1977).

50. Wright, P. D., et al. "Multiple Liquid Phase Epitaxy of $In_{1-x}Ga_xP_{1-z}As_z$ Double-Heterojunction Lasers: The Problem of Lattice Matching," Applied Physics Letters, 31: 40-42 (1 July 1977).

51. IR Industries Technical Information Sheet on PbS Detector TO-2667.

Appendix A: Lattice Matching in the GaInAsP/InP System

Lattice matching occurs when the lattice constant of an epitaxial layer of crystal exactly matches the lattice constant of the substrate on which it was grown. Lattice matching is essential to the production of high-quality heterojunction devices used in modern optoelectronic and microwave technology (Refs 1, 17). Lattice matching between the alloy GaInAsP and an InP substrate is achieved by the opposing effects of adding gallium and arsenic to the InP lattice (Ref 3:1000).

In some epitaxial systems, such as GaInP grown on GaAs, lattice matching is achieved as a result of the minimization of strain and dislocation energies at the epilayer-substrate interface (Ref 22:37). This automatic lattice matching is called "self-matching" (Ref 50:40). GaInAsP grown on InP is not such a self-matching system. Instead, lattice matching between GaInAsP and an InP substrate is a sensitive function of the growth solution composition, the solution supercooling time, and the orientation of the substrate (Ref 22:37).

The lattice constant of $Ga_xIn_{1-x}As_yP_{1-y}$ may be expressed as a function of composition (x and y) and lattice constant (a) by means of the expression

$$a(\mathring{A}) = a(InP) - Ax + By + Cxy \qquad (6)$$

where

$$A = a(InP) - a(GaP)$$
$$B = a(InAs) - a(InP)$$
$$C = a(InP) + a(GaAs) - a(InAs) - a(GaP)$$

For lattice matching to occur between InP (lattice constant of 5.8685 Å) and $Ga_xIn_{1-x}As_yP_{1-y}$, y must be approximately 2.16x (Ref 42:932). To avoid changes in the epilayer's lattice constant during LPE growth, it is necessary to maintain precise temperature control (Ref 42:935). A slight change in temperature can produce a change of lattice constant within an epilayer. Since the composition of GaInAsP epilayers is sensitive to substrate orientation, high-quality epilayers cannot be grown directly on InP substrates that have been thermally etched by vapor loss of P (Ref 22:42). Thermal etching exposes different crystallographic orientations of the substrate, and epilayers grown on the etched substrate develop polycrystalline surface mounds.

It is difficult to determine if a given epitaxial layer of GaInAsP is lattice matched to its InP substrate. Since alloy composition is not necessarily affected by lattice mismatch, chemical analysis is useless (Ref 22:39). Epilayers grown on the [111] crystal face of InP show good morphology regardless of the degree of lattice mismatch (Refs 17:15; 42:936). However, epilayers grown on the [100] crystal face only show good morphology if a high degree of lattice matching exists (Ref 17:15). Cleaved faces of the epilayer are also useless as indicators of lattice mismatch (Ref 22:40). The only dependable method of determining whether lattice mismatch is present is to obtain composite x-ray diffraction patterns with con-

tributions from both the epilayer and the InP substrate (Ref 36:106). These composite patterns can be compared with independent scans of the InP substrate to determine the degree of lattice mismatch.

Vita

Jamie G. G. Varni was born on April 11, 1955 in Sonora, California, the son of James A. Varni and Gladys C. Varni. He graduated from Thomas Downey High School in Modesto, California in 1973. He then attended the University of Southern California in Los Angeles, California, where he obtained a Bachelor of Science degree in Physics in June of 1977. After receiving his commission in June of 1977, Lt. Varni was assigned to the Air Force Institute of Technology in September of 1977.

Permanent Address: 1417 Tully Rd.
Modesto, California 95350

UNCLASSIFIED

SECURITY CLASSIFICATION OF THIS PAGE *(When Data Entered)*

REPORT DOCUMENTATION PAGE		READ INSTRUCTIONS BEFORE COMPLETING FORM
1. REPORT NUMBER AFIT/GEP/PH/78D-14	2. GOVT ACCESSION NO.	3. RECIPIENT'S CATALOG NUMBER
4. TITLE *(and Subtitle)* PHOTOLUMINESCENCE OF GALLIUM INDIUM ARSENIC PHOSPHIDE		5. TYPE OF REPORT & PERIOD COVERED MS Thesis 6. PERFORMING ORG. REPORT NUMBER
7. AUTHOR(s) Jamie G. G. Varni 2Lt		8. CONTRACT OR GRANT NUMBER(s)
9. PERFORMING ORGANIZATION NAME AND ADDRESS Air Force Institute of Technology (AFIT-EN) Wright-Patterson AFB, OH 45433		10. PROGRAM ELEMENT, PROJECT, TASK AREA & WORK UNIT NUMBERS Project No. 2002 Work Unit No. 0128
11. CONTROLLING OFFICE NAME AND ADDRESS AF Avionics Laboratory Wright-Patterson AFB, OH 45433		12. REPORT DATE September 1978 13. NUMBER OF PAGES 92
14. MONITORING AGENCY NAME & ADDRESS*(if different from Controlling Office)*		15. SECURITY CLASS. *(of this report)* Unclassified 15a. DECLASSIFICATION/DOWNGRADING SCHEDULE

16. DISTRIBUTION STATEMENT *(of this Report)*

Approved for public release; distribution unlimited

17. DISTRIBUTION STATEMENT *(of the abstract entered in Block 20, if different from Report)*

18. SUPPLEMENTARY NOTES

Approved for public release; IAW AFR 190-17

JOSEPH P. HIPPS, Major, USAF
Director of Information 19 Jan 79

19. KEY WORDS *(Continue on reverse side if necessary and identify by block number)*

III-V Compounds
Photoluminescence
Gallium Indium Arsenic Phosphide (GaInAsP)
Emission Spectroscopy
Quaternary Compounds

20. ABSTRACT *(Continue on reverse side if necessary and identify by block number)*

A photoluminescent study of high-purity epitaxial GaInAsP was made to determine what impurity and defect levels were present in the epilayers. The samples were excited with an argon-ion laser operating at 4880 Å and 700 mW of power or 4765 Å and 300 mW of power. Luminescence was detected with a cooled PbS photoconductor for sample temperatures from 4.2°K to 100°K. No defect-related peaks were found. The emission

DD FORM 1 JAN 73 1473 EDITION OF 1 NOV 65 IS OBSOLETE

UNCLASSIFIED

20. Abstract continuation:
spectrum of all of the samples was similar, consisting of a narrow, near-band edge peak and a broader peak between 15 meV and 26 meV below the band edge peak. The narrow peak was tentatively identified as being due to free-to-bound recombination. The broad peak was attributed to donor-acceptor pair emission, but no attempt was made to identify the impurities responsible for either peak.